


ORIGINAL RESEARCH

Open Access



# Reinforced HDPE with optimized biochar content for material extrusion additive manufacturing: morphological, rheological, electrical, and thermomechanical insights

Nectarios Vidakis<sup>1</sup>, Markos Petousis<sup>1\*</sup> , Dimitrios Kalderis<sup>2</sup>, Nikolaos Michailidis<sup>3,4</sup>, Emmanuel Maravelakis<sup>2</sup>, Vassilios Saltas<sup>2</sup>, Nikolaos Bolanakis<sup>2</sup>, Vassilis Papadakis<sup>5,6</sup>, Mariza Spiridaki<sup>1</sup> and Apostolos Argyros<sup>3,4</sup>

## Abstract

The development of efficient and sustainable composites remains a primary objective of both research and industry. In this study, the use of biochar, an eco-friendly reinforcing material, in additive manufacturing (AM) is investigated. A high-density Polyethylene (HDPE) thermoplastic was used as the matrix, and the material extrusion (MEX) technique was applied for composite production. Biochar was produced from olive tree prunings via conventional pyrolysis at 500 °C. Composite samples were created using biochar loadings in the range of 2.0–10.0 wt. %. The 3D-printed samples were mechanically tested in accordance with international standards. Thermogravimetric analysis (TGA) and Raman spectroscopy were used to evaluate the thermal and structural properties of the composites. Scanning electron microscopy was used to examine the fractographic and morphological characteristics of the materials. The electrical/dielectric properties of HDPE/biochar composites were studied over a broad frequency range (10<sup>-2</sup> Hz–4 MHz) at room temperature. Overall, a laborious effort with 12 different tests was implemented to fully characterize the developed composites and investigate the correlations between the different qualities. This investigation demonstrated that biochar in the MEX process can be a satisfactory reinforcement agent. Notably, compared to the control samples of pure HDPE, biochar increased the tensile strength by over 20% and flexural strength by 35.9% when added at a loading of 4.0 wt. %. The impact strength and microhardness were also significantly improved. Furthermore, the Direct current (DC) conductivity of insulating HDPE increased by five orders of magnitude at 8.0 wt. % of biochar content, suggesting a percolation threshold. These results highlight the potential of C-based composites for the use in additive manufacturing to further exploit their applicability by providing parts with improved mechanical performance and eco-friendly profiles.

## Highlights

- The reinforcement of MEX 3D printed parts with eco-friendly biochar.
- Biochar was obtained from olive trees.

Handling editor: Wenfu Chen

\*Correspondence:

Markos Petousis

markospetousis@hmu.gr

Full list of author information is available at the end of the article

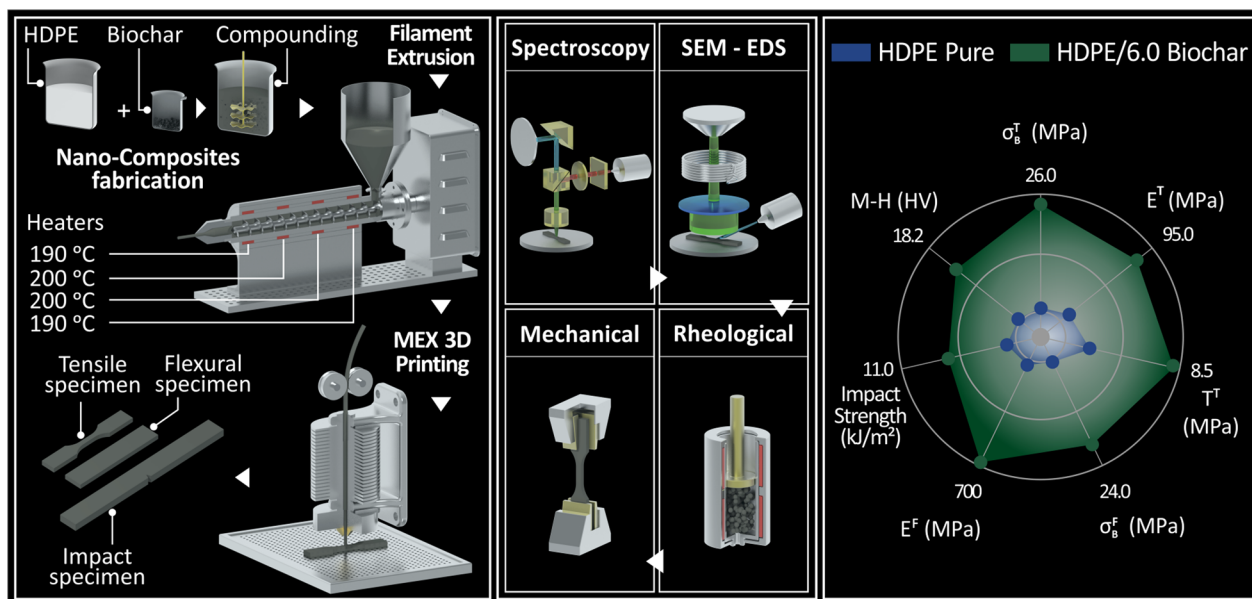


© The Author(s) 2024. **Open Access** This article is licensed under a Creative Commons Attribution 4.0 International License, which permits use, sharing, adaptation, distribution and reproduction in any medium or format, as long as you give appropriate credit to the original author(s) and the source, provide a link to the Creative Commons licence, and indicate if changes were made. The images or other third party material in this article are included in the article's Creative Commons licence, unless indicated otherwise in a credit line to the material. If material is not included in the article's Creative Commons licence and your intended use is not permitted by statutory regulation or exceeds the permitted use, you will need to obtain permission directly from the copyright holder. To view a copy of this licence, visit <http://creativecommons.org/licenses/by/4.0/>.

- Popular high-density polyethylene (HDPE) was the polymeric matrix in the study.
- biochar increased the tensile strength by over 20% and the flexural strength by 35.9% at a loading of 4 wt. %.
- The DC conductivity of the insulating HDPE increased by five orders of magnitude at 8 wt. % biochar loading.

**Keywords** High-density polyethylene, Biochar, Material extrusion 3D printing, Additive manufacturing

### Graphical Abstract



## 1 Introduction

Given the significant waste of resources and environmental damage, society needs to reassess the current development strategies and prioritize environmental protection (Ahmed and Hameed 2020; Beydoun and Klankermayer 2020). Circular bio-economy concepts promote the valorization of residual biomass for the production of novel materials, thus reducing the dependence on non-renewable sources, such as petroleum oil (Väisänen et al. 2017). In this framework, biomass can be converted into a solid, carbon-rich material, called biochar, through pyrolysis. The physicochemical properties of biochar depend on the biomass, pyrolysis temperature, duration, and post-production modification process. To date, biochar has mostly been utilized as a soil improver and its carbon sequestration potential has been established (Lee et al. 2013). There have been reviews of biochar production, characteristics, and uses, particularly as a soil amendment (Lehmann et al. 2011; Meyer et al. 2011; Manyà 2012; Shen and Yoshikawa 2013; Ahmad

et al. 2014). Recently, its potential as a carrier for slow-release fertilizers was demonstrated (Wang et al. 2023). The results of different biochar applications, including agronomy, energy, wastewater treatment, and composite materials, have been summarized by Nanda et al. (2016) and Giorcelli et al. (2019).

Additionally, biochar may be used in industrial applications such as sensors, where only pure carbon materials are used (Noman et al. 2014; Ziegler et al. 2017). There have been significant advances in the use of biochar as a carbon sequestration strategy (Zhang et al. 2018). Prepared from renewable biomass, biochar has an extended porosity, and is rich in carbon (Amalina et al. 2022), so it is frequently used to reinforce plastics. Specifically, it has been reported that biochar can provide greater stability to polymer systems (DeVallance et al. 2015; Nan et al. 2015). However, not all biochars have a positive effect on the mechanical properties of biocomposites (Shah et al. 2023a). According to Das et al. (2015a, b), the carbon content and surface area of biochar are crucial factors

that influence the performance of biochar-based composites, making them extremely promising. According to Tomczyk et al. (2020), increasing the pyrolysis temperature results in biochar with a larger carbon content and an increased specific surface area.

Furthermore, research on carbon-reinforced material composites and their applications in additive manufacturing is rapidly expanding (Ghoshal 2017; van de Werken et al. 2020; Junk et al. 2021; Vidakis et al. 2023a), with research focusing on carbon additives such as carbon nanotubes (Vidakis et al. 2021a, 2021c) and carbon black (Vidakis et al. 2021c, 2021d). However, there is a trend for the use of eco-friendly additives in composites, to improve the performance of polymers in material extrusion (MEX) 3D printing, such as cellulose nanofibers (Vidakis et al. 2021e, 2023b) and glass particles, to improve the performance of polymers (Petousis et al. 2023).

New environmentally-friendly biochar/plastic composite materials have significant potential (Das et al. 2016b; Khan et al. 2017; Giorcelli et al. 2019). Scientists have created composites that use biochar as a filler instead of fibers (Dahal et al. 2019; Matykiewicz 2020; Das et al. 2021). The results showed that the addition of biochar improved the mechanical properties and fire resistance of the composites (Khushnood et al. 2015; Das et al. 2016a, 2017a, b; Ikram et al. 2016; Zhang et al. 2017b). In addition to acting as a filler, biochar considerably improved the processing properties of ultra-high-molecular-weight polyethylene (UHMWPE) (Li and Li 2014).

The advantages of adding biochar to composite materials have been a subject of extensive research (Das et al. 2015c, 2020; Tareq et al. 2019; Zhang et al. 2020a; Mandal et al. 2020; Awad 2021; Wang et al. 2022; Pk et al. 2023). In one study, agricultural biomass wastes, such as corncobs, durian rhizomes, pineapple processing waste, and cassava peels, were selected as raw materials for producing carbon-rich biochar (CRB) using a simple pyrolysis process. The carbon content of CRB generated from cassava rhizomes is enhanced at elevated pyrolysis temperatures. This study also examined the mechanical characteristics of composites prepared by mixing different types of biomass-derived CRB with polylactic acid (PLA). Notably, the composites containing PLA and CRB, which contained more carbon, exhibited improved mechanical properties. Specifically, the addition of CRB powder significantly improved the elastic modulus and impact energy of PLA/CRB composites (Aup-Ngoen and Noipitak 2020).

High-density polyethylene (HDPE) has extensive applications in manufacturing, automotive, packaging, agriculture, and everyday products, owing to its exceptional resistance to heat and cold, chemical stability, mechanical

strength, electrical insulation, and barrier qualities (Musa et al. 2017; Dusunceli and Colak 2008). It is the third most widely used plastic in the world (Kumar et al. 2011). HDPE is the preferred material for fabricating polymer composites because of its flexibility and deformability (Pawlak and Galeski 2005). Recent results have shown that the addition of biochar improves HDPE's dimensional stability and flame resistance of HDPE (Zhang et al. 2020d). Additionally, rice husk biochar has been used to reinforce HDPE, with findings showing a decreased crystallization rate and increased mechanical characteristics (Zhang et al. 2017a). In another study, activated biochar was produced and mixed with HDPE through compounding and injection molding. The addition of activated biochar improved its thermal properties of the activated biochar. The composite with 0.5 wt. % biochar loading possessed the optimum mechanical characteristics, exhibiting exceptional flexural strength (38.66 MPa), flexural modulus of elasticity (2.46 GPa), tensile strength (32.17 MPa), and tensile modulus of elasticity (1.95 GPa), as well as high rigidity, elasticity, creep resistance, and anti-stress relaxation ability. In contrast to this biochar loading, the mechanical characteristics of the composites with 1, 1.5, and 2.0 wt. % biochar loading were inferior compared to pure HDPE. This was attributed to the excess activation agent damaging the porous structure, which affected the performance of the composite (Zhang et al. 2020b).

Based on these considerations, the rationale of this study was to combine biowaste management with material science and manufacturing processes to produce environmentally-friendly composites with improved mechanical properties. The hypothesis is that if a composite has improved mechanical and thermal characteristics, it may be suitable for use in additive manufacturing, thereby improving the environmental profile and sustainability of the process. Herein, for the first time, biochar was used as an additive in a popular HDPE polymer to produce composites with improved mechanical, thermal, and electrical characteristics, in a form compatible with the MEX 3D printing method. The most abundant woody residue in the Mediterranean region used for biochar production was used in the present study. This biochar has not yet been used in additive manufacturing applications. The performance of biofriendly biochar as an additive in MEX 3D printing was evaluated using numerous different types of tests. HDPE was selected as the main component in the manufacturing process (material extrusion and MEX 3D printing). Olive tree pruning, a major woody biomass in the Mediterranean region, was used as the biochar precursor. Olive tree pruning biochar has high carbon content, low ash content, and relatively high

surface area. Other common agricultural residues, such as rice husks, fruit seeds, and maize stems, produce biochar with a higher ash content and lower surface area, both of which are undesirable attributes for polymer reinforcement (Vidakis et al. 2023a). To reinforce the composites, it would be interesting to compare the biochars produced from various woody residues (prunings) of cultivated trees (peach and orange trees) and forest species (pine, oak, and spruce). The scientific gap covered by this study is related to the development of composites with improved performance for the MEX 3D printing method using HDPE as the matrix material. HDPE is used in a wide range of applications; therefore, the introduction of a composite with improved performance is advantageous, particularly for eco-friendly materials. Composites with improved characteristics are sought after in the industry, particularly for 3D applications, because they contribute to expanding the field of applications.

The Mediterranean region has an abundance of this renewable waste, which is currently underutilized. To minimize the volume and stop the spread of infection, olive tree pruning is traditionally burned in the open on an annual basis in large quantities. However, organic aerosols in the Mediterranean region and CO<sub>2</sub> emissions are greatly increased by this approach. Previous research has revealed that the open burning of pruning damaged the soil structure and increased the likelihood of flames in adjacent areas (Kostenidou et al. 2013; García Martín et al. 2020; Romero-García et al. 2022). Given that an estimated 33 million tons of olive tree pruning are generated annually, most of which occurs in the Mediterranean region, the potential for carbon sequestration by converting this biomass to an added value, the carbon product, is high (Cuevas et al. 2019). Therefore, if the addition of olive tree pruning biochar improves the thermomechanical characteristics of additive manufacturing polymers, it may provide an alternative exploitation pathway for this agricultural waste. Additionally, owing to the carbon-based nature of biochar, it is expected to modify its electrical properties, providing an additional asset for the prepared HDPE/biochar composites. The electrical properties of polymer nanocomposites based on carbon additives, such as carbon black, graphite, carbon nanotubes, and nanofibers, have been thoroughly studied, and conductive composites with low filler contents have been prepared. The enhanced electrical behavior of such composites at low filler contents was interpreted based on the percolation theory (Brigandi et al. 2014; Gulrez et al. 2014).

The objectives of this work were to:

- a) evaluate biochar as an alternative, sustainable, and eco-friendly additive for polymeric matrices in MEX 3D printing;
- b) improve the performance of HDPE in MEX 3D printing by developing corresponding composites;
- c) compare the performance of biochar in the HDPE composites with other polymeric matrices;
- d) compare the performance of biochar with other fillers;
- e) combine biochar and HDPE into a mixture and apply a thermomechanical extrusion procedure;
- f) investigate the mechanical and thermal properties of the 3D-printed specimens ;
- g) fully characterize the composites by conducting Raman, rheological, and electrical studies;
- h) assess the samples' morphological characteristics with Scanning electron microscopy (SEM);
- i) correlate the measured qualities of the composites and find connections between them.

## 2 Materials and methods

Figure 1 shows the experimental steps, starting from the raw materials, filament production, specimens, mechanical tests, and analysis of the results. Initially, the raw materials were dried, followed by the extrusion and drying of the filament, quality control, and characterization and testing of filament properties. Subsequently, the specimens were fabricated and subjected to various mechanical tests, followed by rheological analysis and morphological characterization.

### 2.1 Materials

The matrix material was Kritilen High-Density Polyethylene polymer (Plastika Kritis S.A., Heraklion, Greece) in powder form (industrial grade). According to the supplier, its density was 0.960 g cm<sup>-3</sup>, mass-flow rate was 7.5 g 10 min<sup>-1</sup> and Vicat softening temperature was 127 °C. The biochar was produced by flame-curtain pyrolysis of olive tree prunings (collected in Chania, Greece) at a temperature of 500 °C. Detailed information regarding the production conditions, materials, dimensions, and other specifications of the pyrolysis kiln can be found in the literature (Tsubota et al. 2021). Following production, the biochar was ground in a Sepor-type rod mill and the < 100 µm fraction was collected for use. The basic properties of the biochar are listed in Additional file 1: Table S1. The full characterization of biochar can be found in our previous study (Vidakis et al. 2023a).

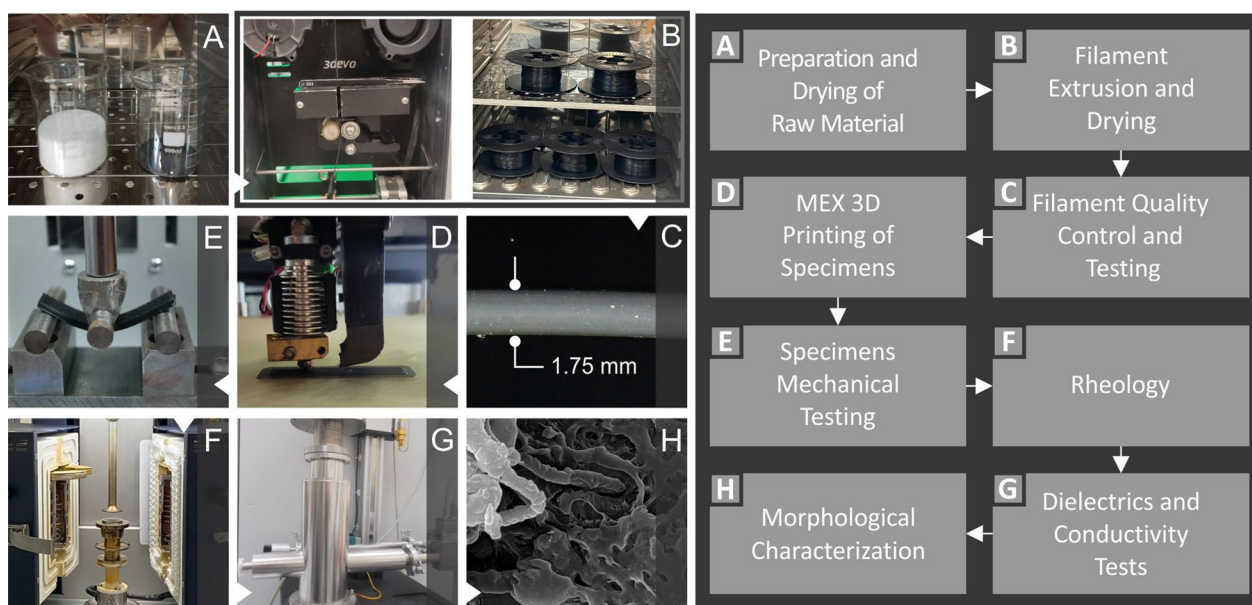


**Fig. 1** Presentation of the experimental methodology: **A** preparation of the raw materials, **B** filament production and drying, **C** quality control of filament, **D** fabrication of 3D-P specimens through MEX, **E** testing of specimens' mechanical properties, **F** rheology analysis, **G** dielectric and conductivity tests and **H** morphological characterization of specimens

## 2.2 Methods

### 2.2.1 Preparation of HDPE-biochar composites

HDPE and biochar were thoroughly dry-mixed in their raw form using a high-wattage blender at 4000 rpm for 30 min, followed by drying and fabrication into filaments. Biochar was added to the HDPE matrix at the loadings of 2.0, 4.0, 6.0, 8.0, and 10.0 wt. %. The raw materials were dry-mixed and no other additives were added to each mixture.

The biochar concentration in the matrix was gradually increased. The samples were prepared and tested for each loading. At loadings higher than 6.0 wt. %, the mechanical properties rapidly decrease in the samples, indicating the saturation of the biochar in the HDPE matrix. Therefore, there was no further increase in the biochar loading in the matrix beyond 10.0 wt. %. The saturation of fillers in polymer matrices has been extensively reported, which negatively affects the mechanical properties of the composites (Mazzanti et al. 2019). The filament extrusion was conducted at a 3D Evo Precision 450, 3D Evo B.V. (Utrecht, The Netherlands), with an average of 1.75 mm filament diameter, in order to be suitable for the fabrication of the specimens.

### 2.2.2 Raman spectroscopy, thermogravimetric analysis, differential scanning calorimetry, and rheological properties

Spectroscopic measurements of Raman signals were performed under laboratory conditions. A confocal

LabRAM HR Raman spectrometer (HORIBA Scientific, Kyoto, Japan) was used. The laser module operated at a central wavelength of 532 nm and delivered a power of 90 mW. To attenuate the laser power incident on the sample, a 5% Neutral Density filter was employed in the optical path. Sample excitation and imaging were achieved with a microscope 50×Olympus objective lens (LMPlanFL N, Tokyo, Japan) with a Numerical Aperture (NA) and a 10.6 mm working distance. The acquisition settings were as follows:

- measurement spectral ranged from 50 up to 3900  $\text{cm}^{-1}$
- Raman spectral resolution was around 2  $\text{cm}^{-1}$
- imaging resolution was 1.7  $\mu\text{m}$  laterally and 2  $\mu\text{m}$  axially
- exposure time per point was 10 s and in each point
- 5 accumulations per point.

The laser power applied to the sample surface was 2 mW. All the measured areas were visually inspected after irradiation using a microscope to ensure no discoloration or degradation.

The thermal stability and properties of the fabricated composites were investigated by thermogravimetric analysis (TGA) using a Perkin Elmer Diamond TGA/DTGA device (Perkin Elmer, Waltham, United States). The temperature ramp was 10  $^{\circ}\text{C min}^{-1}$ , and the temperature ranged from 40  $^{\circ}\text{C}$  to 550  $^{\circ}\text{C}$ . Differential scanning

calorimetry (DSC) was also performed with the assistance of a DSC 25 (TA Instruments, New Castle, United States) apparatus, with experimental temperatures ranging between 30 °C and 200 °C.

Based on the rheological properties, we referred to the viscosity and melt flow rate (MFR) values. These measurements are important for quantifying how the introduction of the filler changes the behavior of the matrix. First, rheological experiments were conducted to measure the viscosity of the material when the composite was heated to the printing temperature. From these measurements, shear thinning behavior can be observed as the viscosity decreases as the shear rate increases, which is a favorable property for materials intended for MEX 3D printing applications. The shear-thinning behavior helps make the material more viscous when the material has been deposited, thus maintaining its shape. In addition, at higher shear rates, the material flows more easily, as observed by the lowering of the viscosity values at higher shear rates, which helps prevent nozzle clogging and the development of buckling phenomena in the printed part. All of the above are also in correlation with the MFR measurements, from which we can obtain a better understanding of the material’s behavior when flowing through a hole, which is a process similar to the flow of the material through the printer’s nozzle during the MEX 3D printing process. Experiments were conducted using a DHR-20 Discovery Hybrid Rotational Rheometer (TA Instruments, New Castle, DE, USA). This rheometer

had a parallel plate configuration with a diameter of 25 mm and was equipped with a temperature-controlled environmental test chamber. To prevent overheating and sample damage, each data point was subjected to a 20-s acquisition time limit. In addition to rotational rheometry, melt flow rate (MFR) measurements were conducted according to international standards (ASTM D1238-13).

**2.2.3 Mechanical tests**

Both tensile and flexural strength tests were conducted on an Imada MX2 (Imada Inc., Northbrook, Illinois, USA) motorized test stand according to the ASTM D638-14 (type V) and ASTM D790-10 standards, respectively. The Charpy notched impact test was performed using a Terco MT220 apparatus (Terco AB, Kungens, Sweden) following the ASTM D6110 standard. Vickers microhardness was measured using an Inova Test 300-Vickers instrument (Innovatest Europe BV, Maastricht, The Netherlands) following the ASTM E384-17 standard. Figure 2 presents the MEX 3D printing (3D-P) parameters, along with the samples from the fabricated tensile, flexural, and Charpy notched specimens, as well as an illustration of their form and dimensions. The nozzle and bed temperatures were set at 230 °C and 90 °C, respectively, while the layer thickness was set at 0.2 mm and the travel speed was 40 mms<sup>-1</sup>. The 3D printing settings were selected according to the preliminary testing of the MEX 3D printing process with specific composites and by consulting the corresponding research on the MEX 3D printing process of

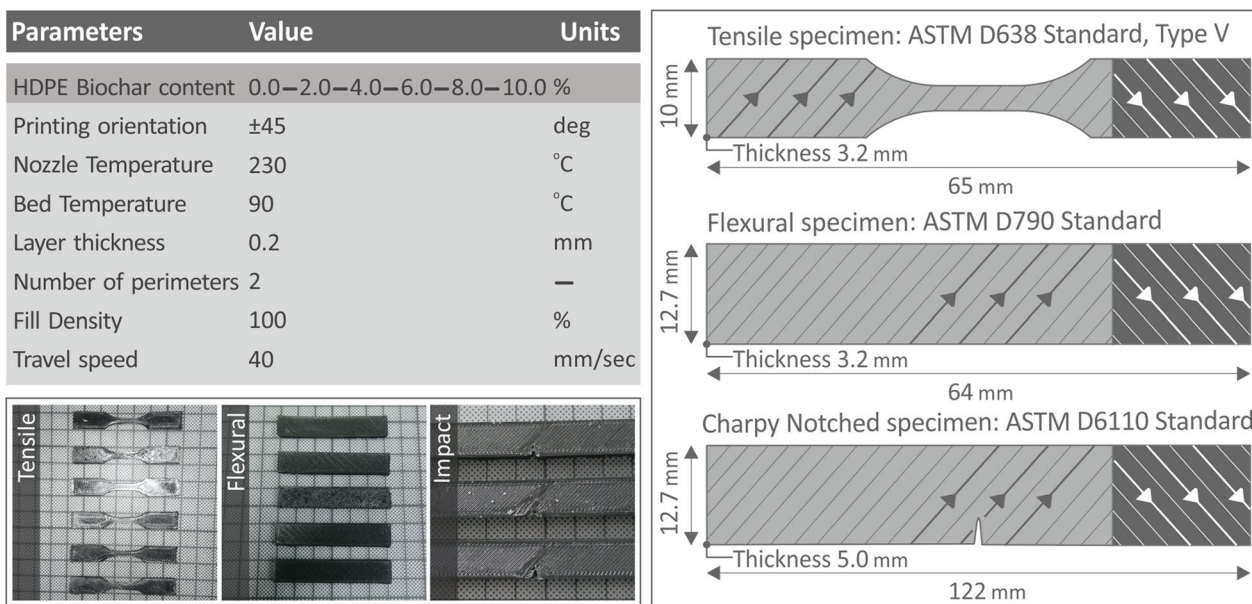


**Fig. 2.** 3D Printing parameters, samples of the 3D printed specimens, and illustration (on the right side) of each specimen’s geometry and dimensions corresponding to every mechanical test (ASTM D638, D790, and D6110 standards)

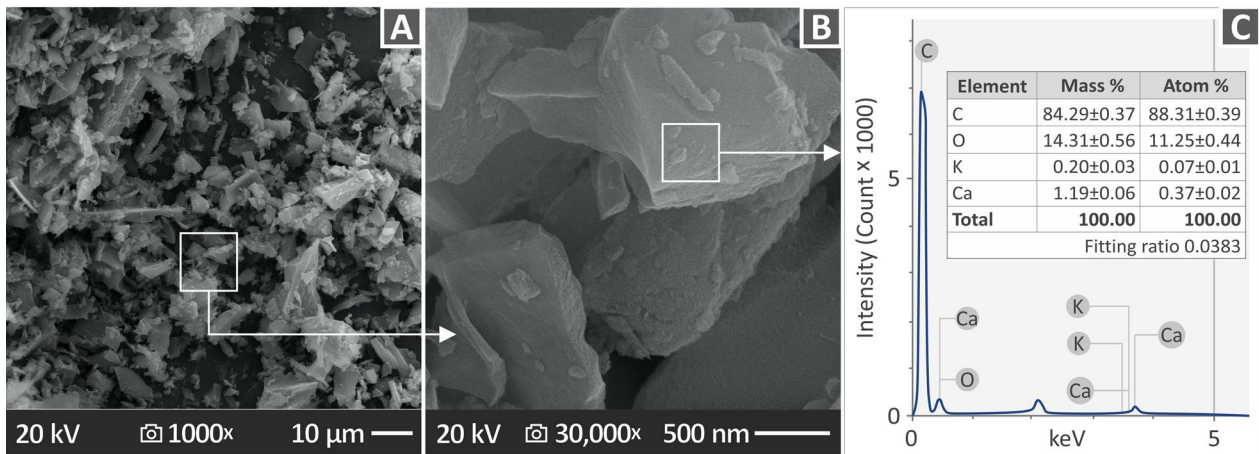


**Fig. 3** Biochar SEM images at **A** 1000× and **B** 30,000× magnification, and **C** chemical analysis graph of biochar through EDS mapping

the HDPE polymer (Vidakis et al. 2021b, 2022a). In all tests, five specimens were tested for each biochar loading and test. All tests were conducted at room temperature of approximately 23 °C and humidity of 55%.

#### 2.2.4 Scanning electron microscopy and energy dispersive spectroscopy analysis

Scanning electron microscopy (SEM) and Energy-dispersive X-ray spectroscopy (EDS) analyses of the biochar were performed using an SEM JSM-IT700HR (Jeol Ltd., Tokyo Japan) device. Figure 3A and B present SEM images of the biochar captured at 1000× and 30,000× magnification, respectively. Figure 3C shows the EDS analysis, where carbon (C), oxygen (O), potassium (K), and calcium (Ca) are the elements. C was found to have the highest levels, which is reasonable because biochar is a carbon-rich material (Richard et al. 2016). Images were also captured from both the fracture and side surfaces of the specimens at various magnifications to evaluate the morphology of the 3D printing structure and fracture surface, respectively.

#### 2.2.5 Broadband dielectric spectroscopy (BDS)

Electrical/dielectric measurements were performed using a high-resolution spectrometer (Alpha-ANB dielectric analyzer, Novocontrol Technologies, Montabaur, Germany) equipped with a ZGS Alpha Active sample holder in conjunction with a BDS 1100 unit, which ensures low-noise and accurate and repeatable measurements over a broad frequency range. WinDeta software was used for system control and data acquisition (Saltas et al. 2013). A two-electrode configuration was used, where each disk-shaped specimen (40 mm in diameter and 4 mm thick)

was considered the dielectric material of the sandwich-structured capacitor. Conductive Ag paste was applied on both sides of the specimens to achieve stable electrical contact with the gold-plated electrodes of the sample holder. Each spectrum was obtained over a wide frequency range of the applied AC electric field, that is, from  $10^{-2}$  to  $4 \times 10^6$  Hz. All measurements were performed at room temperature (25 °C).

The dielectric material of the capacitor is equivalent to an electrical circuit consisting of a resistance  $R(\omega)$  in parallel with capacitance  $C(\omega)$ . These quantities are the output values of the analyzer and are used to represent the dielectric data at different formalisms, such as the dielectric permittivity  $\epsilon^*(\omega)$ , complex impedance  $\sigma^*(\omega)$ , and loss factor  $\tan(\delta)$ . The real part  $\epsilon'^{\wedge}$  of the complex permittivity is a direct measure of the energy storage in the material owing to the applied electric field, whereas the imaginary part  $\epsilon''$  is associated with the energy loss within the material. The above quantities are related to each other by the following relationship:

$$\epsilon^*(\omega) = \epsilon' - i\epsilon'' = \frac{C(\omega)}{\epsilon_0 \pi r^2 / d} - i \frac{1}{\omega R(\omega) \epsilon_0 \pi r^2 / d} \quad (1)$$

$$\tan(\delta) = \frac{\epsilon''}{\epsilon'} \quad (2)$$

$$\sigma^*(\omega) = \sigma' - i\sigma'' = i\omega\epsilon_0(\epsilon^*(\omega) - 1) = \omega\epsilon_0\epsilon'' - i\omega\epsilon_0(\epsilon' - 1) \quad (3)$$

where  $d$  is the distance between the electrodes of radius  $r$ ,  $\omega = 2\pi f$  is the angular frequency and  $\epsilon_0$  is the permittivity of the vacuum.

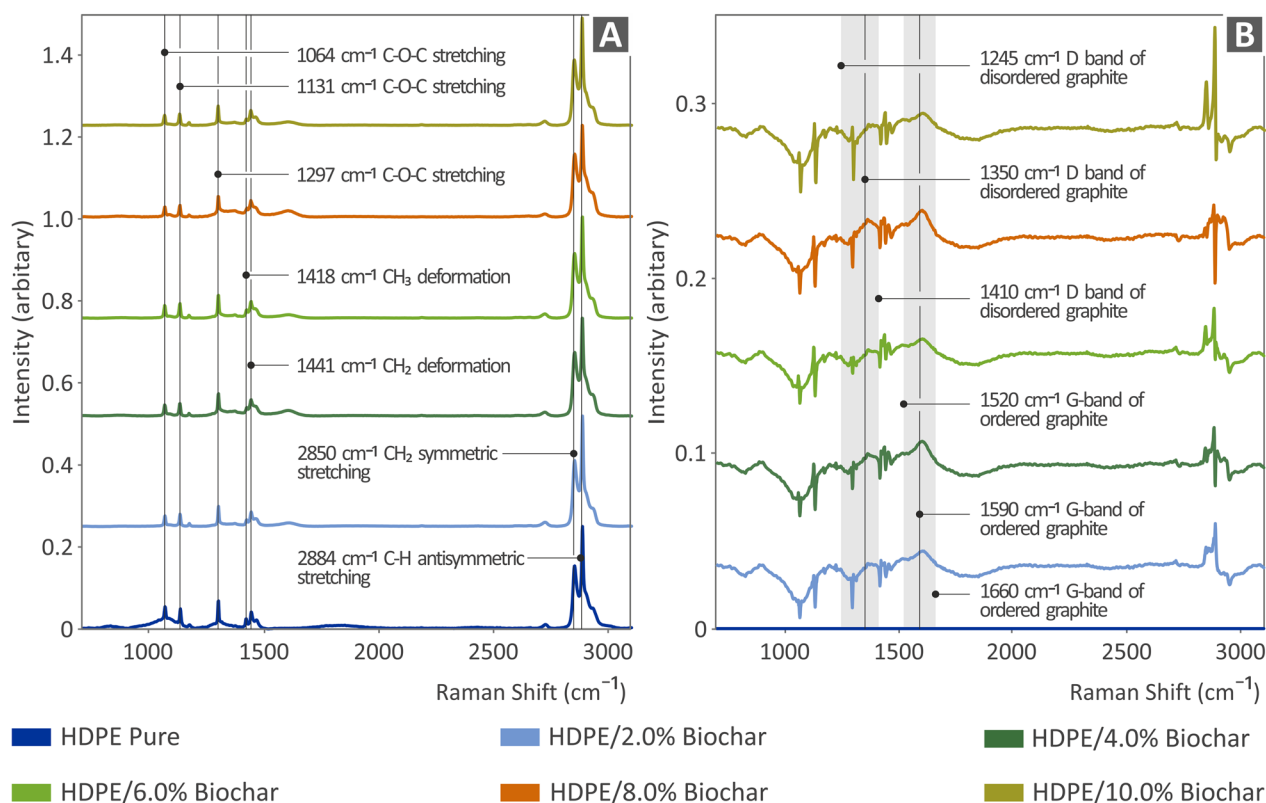


**Fig. 4** **A** Raman analysis results of pure HDPE and all HDPE/ biochar composites (2.0, 4.0, 6.0, 8.0, and 10.0 wt. %), and **B** results from the subtraction of pure HDPE from all HDPE/ biochar composites

### 3 Results

#### 3.1 Characterization

Figure 4A and B show the Raman spectra of pure HDPE and HDPE/biochar composites prepared at all biochar loadings (2.0, 4.0, 6.0, 8.0, and 10.0 wt. %), as well as the spectra after subtraction of pure HDPE from all HDPE/ biochar composites. To avoid any errors introduced by subtraction, the spectral information obtained from the subtracted signals was filtered by the expected Raman signals of the biochar component addition, as well as by the linear correlation of the wt. % concentration. The Raman peaks of the pure HDPE sample were identified and compared with those reported in the literature, and are presented in Additional file 1: Table S2.

As shown in Fig. 4A, the Raman peaks identified in all samples belong to pure HDPE. In particular, C–O–C stretching was observed at 1064, 1131, and 1297  $\text{cm}^{-1}$ .  $\text{CH}_3$  and  $\text{CH}_2$  deformations were observed at 1418 and 1441  $\text{cm}^{-1}$ , respectively. Moreover,  $\text{CH}_2$  symmetric stretching was observed at 2850  $\text{cm}^{-1}$  and C–H antisymmetric stretching at 2883  $\text{cm}^{-1}$ .

The addition of biochar presented only two peaks, one between 1245 and 1410 with a central wavelength at 1350

$\text{cm}^{-1}$ , which is the graphite D band of disordered graphite, and the second between 1520 and 1660  $\text{cm}^{-1}$  with a central wavelength at 1590  $\text{cm}^{-1}$ , which is the G-band of ordered graphite. These large peaks grew as the concentration of biochar increased and were present more at 8.0 wt. % and 10.0 wt. % loadings. This representation of the D and G bands of the graphite structure in the biochar was in accordance with that reported in the literature (Li et al. 2019; Sousa et al. 2020).

#### 3.2 Thermogravimetric and differential scanning calorimetry analyses

Figure 5A and B show graphs of the weight loss and heat flow with the temperature of pure HDPE and all HDPE/ biochar composites. As shown in Fig. 5A, pure HDPE started to lose weight at lower temperatures than the biochar-filled composites, whereas acute weight loss occurred at similar temperatures for both the HDPE and HDPE/biochar composites. This suggests that the addition of biochar did not compromise the thermal stability of the pure HDPE. Additionally, the residual weight after the measurements agreed with the biochar loading in all



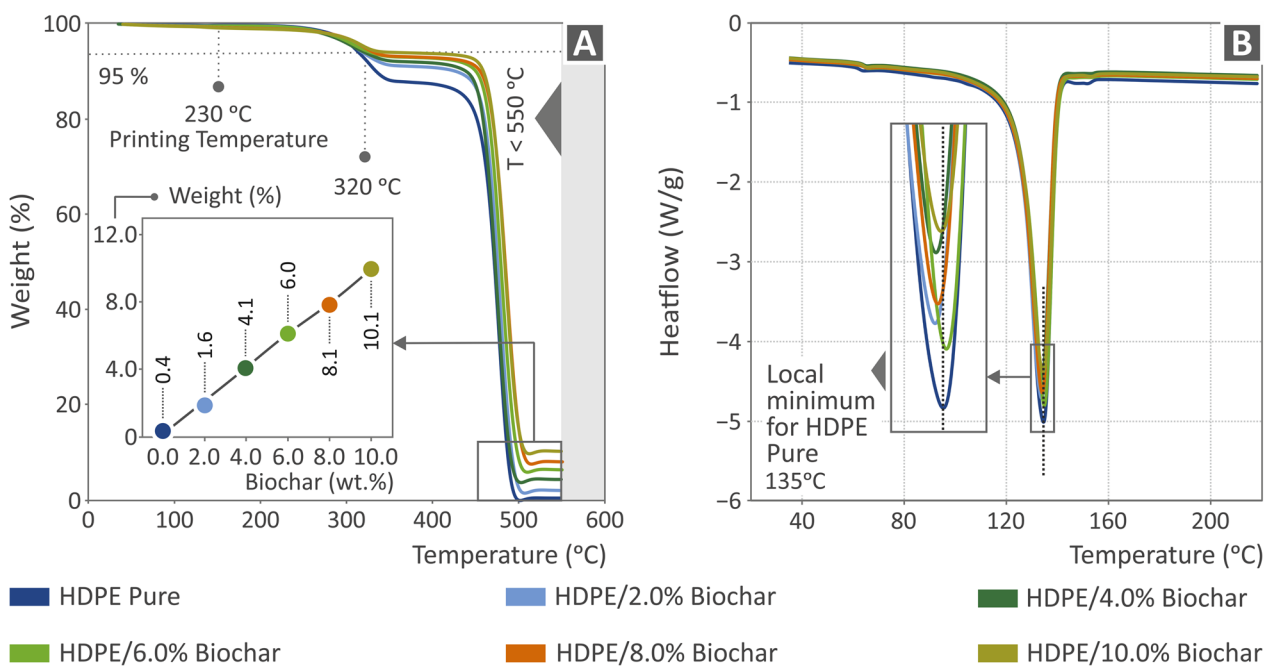


**Fig. 5** Pure HDPE and all HDPE/ biochar composites (2.0, 4.0, 6.0, 8.0, and 10.0 wt. %) **A** TGA graph, **B** DSC graph

the composites, as shown in the inset of Fig. 5A. Figure 5B shows that, only in the case of HDPE/ 6.0 wt. % biochar the heat-flow presented a higher value than pure HDPE and overall no significant differences can be observed in the curves produced during the DSC measurements for the pure HDPE and the HDPE/biochar composites. A possible reason for the previous observation is that as

the amount of filler increases, the weight percentage of the matrix decreases, and as a result, smaller amounts of energy are required to melt the same weight of the composite material. However, a further increase in the filler percentage can result in the entanglement of the polymer chains, thus requiring greater amounts of energy to melt the composite material.

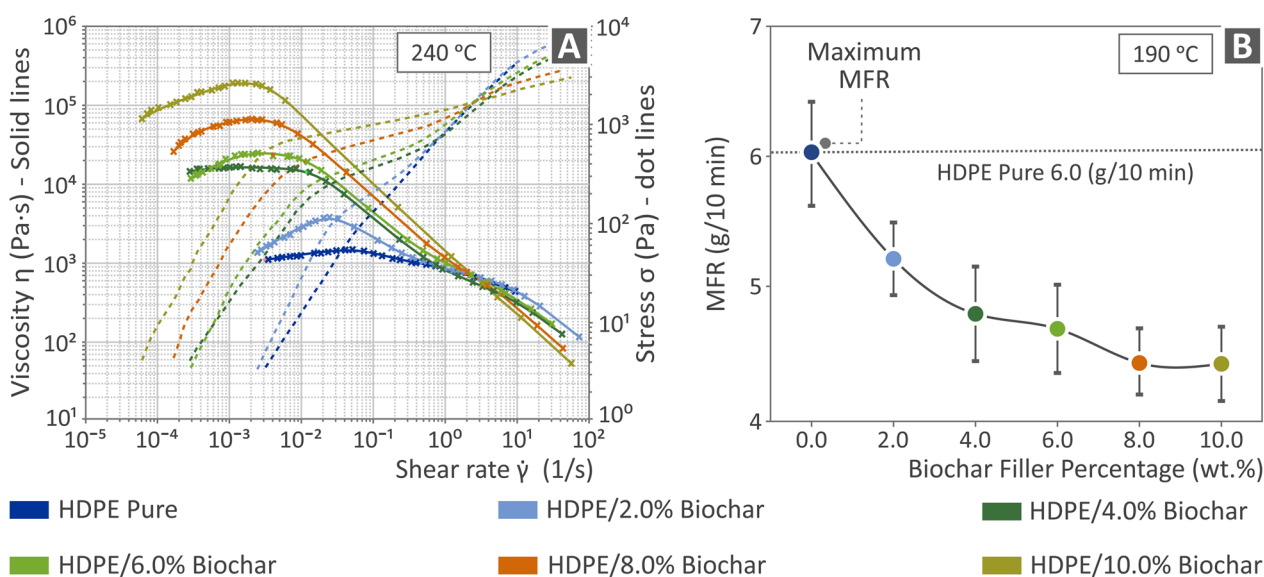


**Fig. 6** **A** Viscosity and shear rate of HDPE and HDPE-biochar composites, and **B** maximum flow rate versus biochar loading

### 3.3 Viscosity and melt flow rate analyses

Figure 6 shows a graph of viscosity and stress as to shear rate at 240 °C (Fig. 6A) and melt flow rate (MFR) as to biochar loading at 190 °C (Fig. 6B), regarding HDPE pure and all HDPE/ wt. % biochar composites. As shown in Fig. 6A, as the biochar loading quantity increased, both viscosity and stress increased. In contrast, the maximum melt flow rate (MFR) was determined for pure HDPE and was reduced by increasing biochar loading, as shown in Fig. 6B. Such differences in the rheological properties of the composites can affect the processability of the materials during filament extrusion and 3D printing as well as the overall quality and performance of the produced samples.

### 3.4 Electrical/dielectric measurements

The electrical/dielectric properties of the pure HDPE and HDPE/biochar composites at various filler concentrations (2.0, 4.0, 6.0, 8.0, and 10.0 wt. % of biochar) are depicted in Fig. 7A–D. The real part of the dielectric permittivity ( $\epsilon'$ ) of HDPE in the measured frequency range exhibited three distinct regions. A step-like behavior

was observed at  $\sim 2 \times 10^4$  Hz, where  $\epsilon'$  increases gradually from the value of 2.4 measured at high frequencies to 3.5 in the mid-frequency range. This observed behavior manifests as a broad peak at approximately  $10^4$  Hz in the  $\tan(\delta)$  representation and as a conductivity relaxation peak in the conductivity spectrum. This feature is attributed to  $\alpha$ -relaxation owing to the motion of the chains within the crystalline phase of HDPE (Suljovrujic et al. 2013). At the low-frequency region, i.e., below 1 Hz, a monotonic increase of  $\epsilon'$  is observed due to ionic conductivity superimposed by the contribution of  $\delta$ -relaxation (Li et al. 2020). The DC plateau observed at low frequencies in the conductivity spectrum of pure HDPE (Fig. 7C) corresponds to a dc-conductivity value of the order of  $10^{-13}$  S/cm. This value is in good agreement with the reported values, suggesting the insulating behavior of the pure sample (Krupa et al. 2004; Linares et al. 2008; Gabhi et al. 2017).

The conductivity spectrum of pure biochar in the compressed powder form is shown in Fig. 7C. High constant conductivity values were measured ( $\sim 2 \times 10^{-4}$  S  $\text{cm}^{-1}$ ) over almost the entire frequency range, which implies a

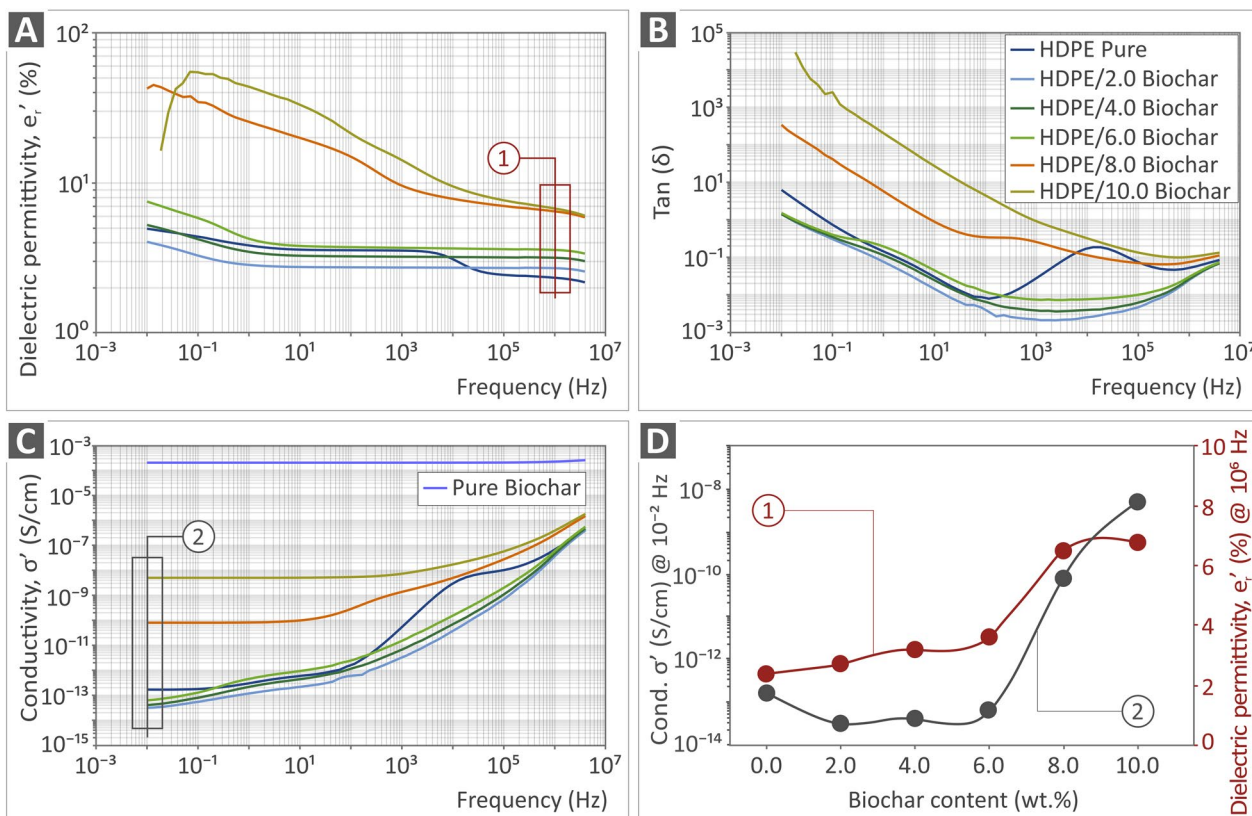


**Fig. 7** A the real part of dielectric permittivity,  $\epsilon'$  B dielectric losses,  $\tan(\delta)$  and C real part of complex conductivity  $\sigma'$ , as a function of frequency, of pure HDPE and HDPE/biochar nanocomposites at different biochar concentrations. D dc-conductivity and dielectric permittivity  $\epsilon_\infty$  as a function of biochar filler content

good electrical behavior of the filler. The reported conductivity values of biochar samples may vary by more than six orders of magnitude, that is, from  $10^{-6}$  S  $\text{cm}^{-1}$  to a few hundred S  $\text{cm}^{-1}$ , depending on the carbon content and the heat treatment process of the samples (Gabhi et al. 2017). In this study, the low-carbon content (76.7 wt. %) of the biochar sample (Vidakis et al. 2023a) results in relatively low values in the measured ac-conductivity spectrum.

When the filler content is increased to 6.0 wt. %, the recorded dielectric and conductivity spectra appear almost identical in shape but with small differences in the absolute values of both dielectric permittivity and ac-conductivity, over the entire measured frequency range. Remarkably, the  $\alpha$ -relaxation band disappeared upon the addition of the filler, a finding that has been reported for structural incorporation into polymer matrix chains (Suljovrujic et al. 2013). A further increase in the biochar content to 10.0 wt. % causes abrupt changes in the measured quantities by orders of magnitude in the low-frequency region, as clearly indicated in Fig. 7D where dc-conductivity and  $\epsilon_{\infty}$  are shown as a function of filler content. Specifically, the DC conductivity increases from

$3 \times 10^{-14}$  S  $\text{cm}^{-1}$  to  $5 \times 10^{-9}$  S  $\text{cm}^{-1}$  and  $\epsilon_{\infty}$  from 2.3 to 6.8 at 10.0 wt. % of biochar content. This finding suggests the existence of a percolation threshold, above which the conductivity rapidly increases to high values owing to the formation of a conductive network of filler nanoparticles, which is consistent with the reported cases of carbon-based polymer nanocomposites (Brigandi et al. 2014; Gulrez et al. 2014).

### 3.5 Monitoring of filament diameter and testing

Figure 8A and C show the microscopic examination and inspection of the diameters of the HDPE and HDPE-biochar composites. Two different filament segments were observed for pure HDPE and the composite. There are no defects or voids observed at either of the filaments, while their diameter is steadily ranging between 1.65 mm and 1.85 mm. Figure 8B shows the results from the tensile strength test conducted on the filaments, with the highest value of 32.9 MPa determined for the HDPE/4.0 wt. % biochar filament (32.9 % above pure HDPE). Similarly, the optimum tensile modulus of elasticity was obtained for HDPE/4.0 wt. % biochar (26.0 % above pure HDPE). It should be noted that, to the authors'

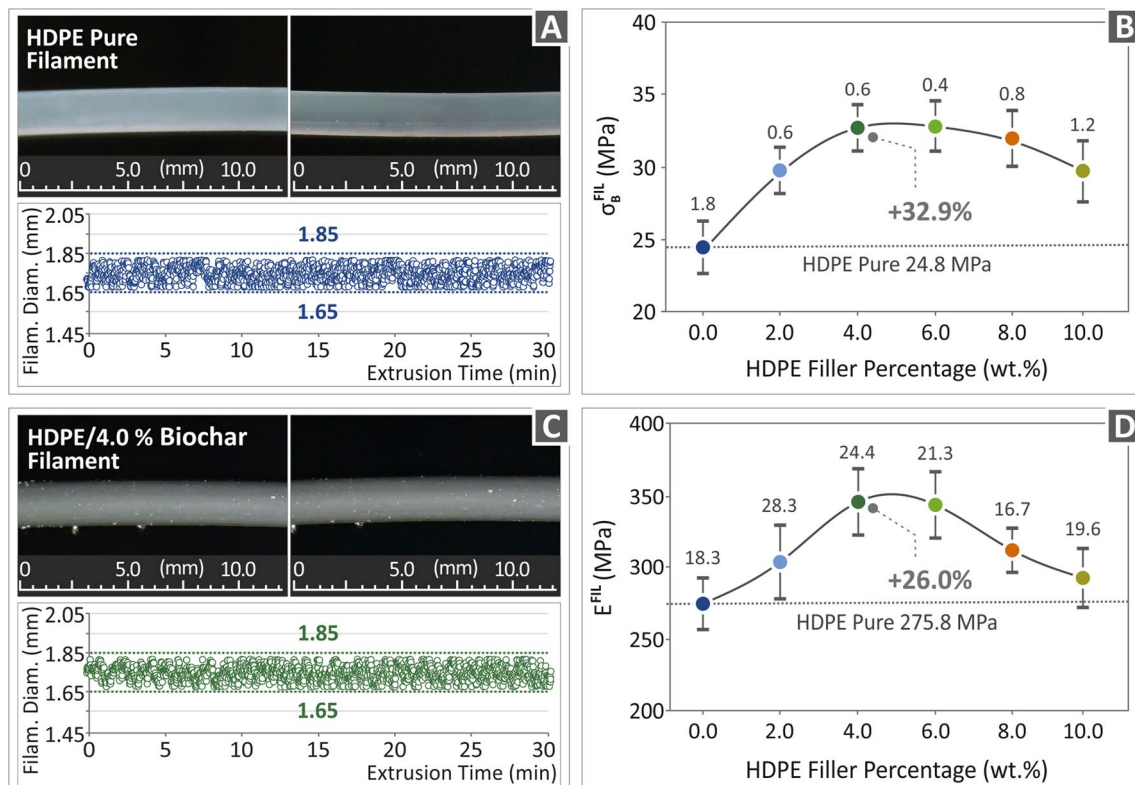


**Fig. 8** **A** Microscopy examination and diameter inspection of the fabricated HDPE pure filament, **B** filament tensile strength to strain, **C** microscopy examination and diameter inspection of the fabricated HDPE/4.0 wt. % biochar filament, and **D** tensile modulus of elasticity of HDPE and HDPE-biochar composites

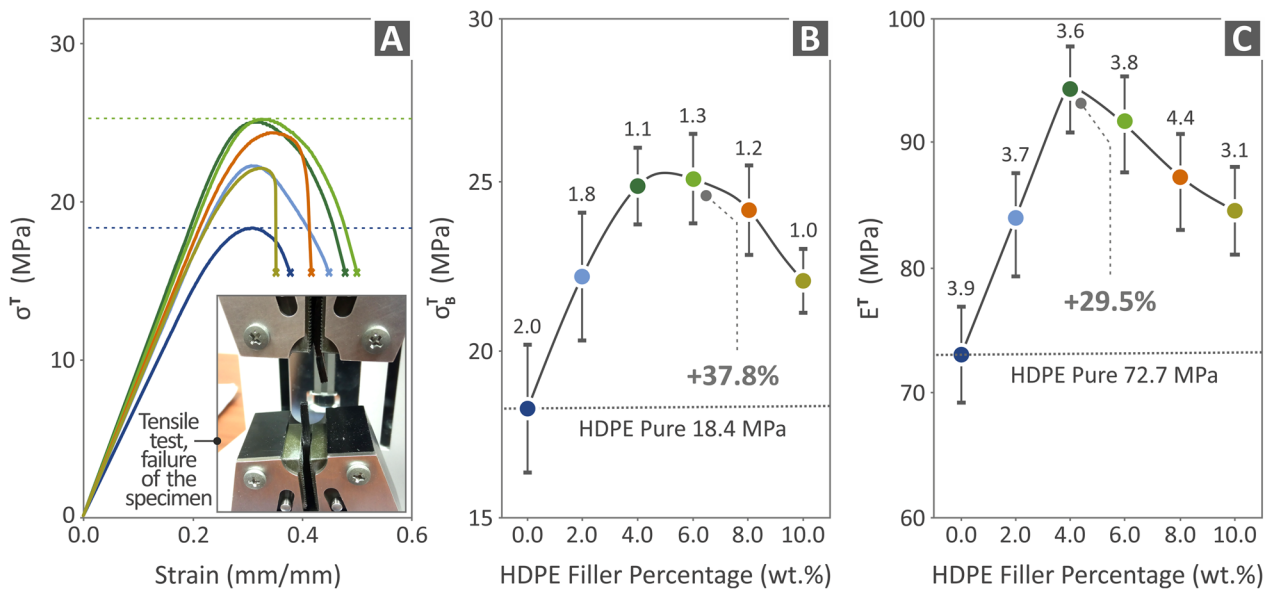


**Fig. 9** Results from the specimens' tensile tests (pure HDPE and all HDPE/ biochar composites, i.e., 2.0, 4.0, 6.0, 8.0, and 10.0 wt. %) **A** tensile stress to strain, **B** tensile strength, and **C** tensile modulus of elasticity

best knowledge, no standard exists for the mechanical testing of such filaments. Therefore, the results of the tensile tests of the filaments could not be directly compared with the corresponding results for the 3D-printed samples. These experiments indicated the strength of the solid material and the reinforcement trend with the addition of filler.

### 3.6 Testing of specimens' mechanical properties

Figure 9A shows a graph of tensile stress versus strain, along with an image from the tensile testing of one randomly chosen specimen. At all biochar loadings, the tensile stress was higher than that of the pure HDPE. With the exception of the 10.0% wt, all the HDPE-biochar composites failed at higher strain values, indicating a

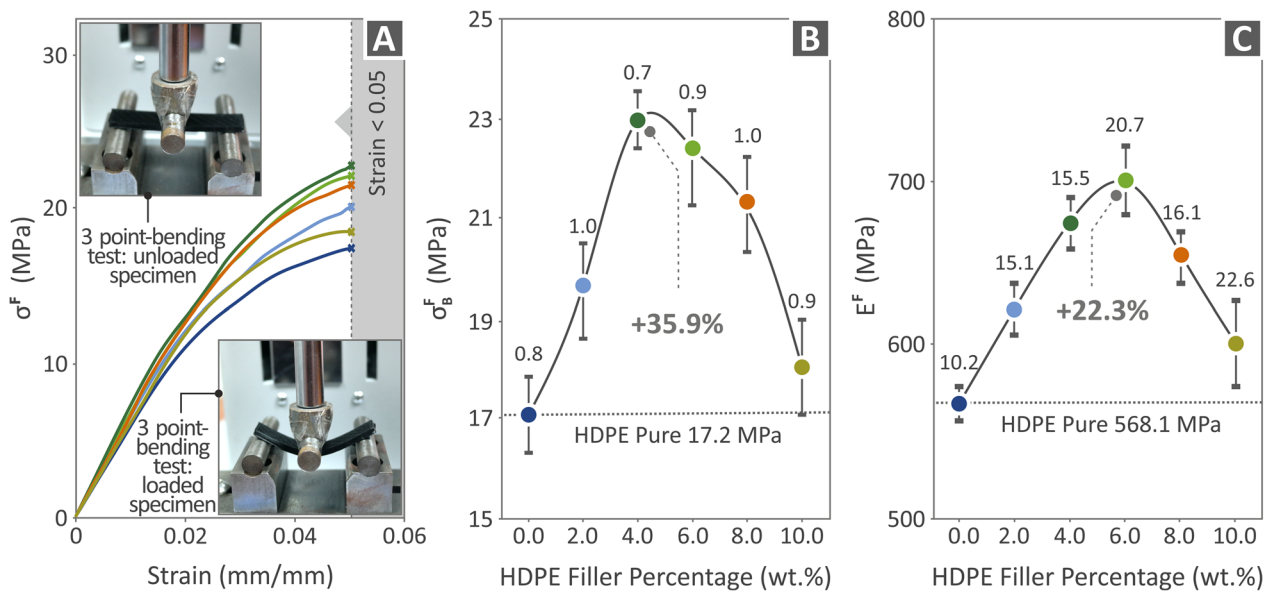


**Fig. 10** Results from the specimens' flexural tests (pure HDPE and all HDPE/ biochar composites, i.e., 2.0, 4.0, 6.0, 8.0, and 10.0 wt. %) **A** flexural stress to strain, **B** flexural strength, and **C** flexural modulus of elasticity

more ductile response than that of pure HDPE. Figure 9B shows the dependence of the tensile strength on the biochar loading. The 6.0 wt. % HDPE-biochar composite showed the highest value of 25 MPa, 37.8% above the pure HDPE value. With respect to the tensile modulus of elasticity, the composite with 4.0 wt. % biochar had the highest value of 95 MPa, which corresponded to a 29.5% increase compared to the respective value for pure HDPE.

The effect of biochar addition on the composite was also evident in the flexural stress measurements (Fig. 10A). At all biochar loadings, the flexural stress values were higher than those obtained from pure HDPE, whereas the 4.0 wt. % biochar composite showed the optimum flexural stress behavior. It should be noted that the experiment was terminated at 5% strain in accordance with the ASTM D790 standard, without the samples having failed in the flexural test. Figure 10B shows the flexural strength results for all composite samples. A composite with 4.0 wt. % biochar-HDME composite exhibited the highest flexural strength of 23 MPa, corresponding to 35.9% above the pure HDPE value. The flexural modulus of elasticity of the 6.0 wt. % biochar-HDME showed the highest response among the samples tested.

The tensile toughness results of the composites are shown in Fig. 11A. The toughness metric represents the energy absorbed by the material during mechanical testing. It is calculated as the integral of stress versus strain. This parameter can be valuable in the design process to

estimate the fracture resistance of a material. An optimum value of  $8.5 \text{ MJ m}^{-3}$  was obtained for the composite containing 6.0 wt. % biochar. The addition of biochar also had a major influence on the Charpy impact strength, with a 2.0 wt. % biochar-HDPE composite achieving a value 28.5% larger than the pure HDPE. The microhardness of the composites showed a linear dependence on the biochar loading, reaching a maximum value of 18 HV at 10.0 wt. % biochar-HDPE sample (9.1% increase compared to the respective value for the pure HDPE).

### 3.7 Evaluation of 3D-P specimens through SEM analysis

The HDPE-biochar composites in this study were subjected to scanning electron microscopy (SEM), and the images captured at various magnifications are presented in Figs. 12, 13. Figure 12A, B, and C show the SEM images of pure HDPE at 150× magnification of the side surface and 25× and 1000× magnifications of the fractured surface. Figure 12D, E, and F show SEM images of HDPE/ 4.0 wt. % biochar at 150× magnification of the side surface, and 25× and 1000× magnification of the fractured surface. Figure 12G, H, and I present the SEM images captured by the HDPE/ 8.0 wt. % biochar specimens at 150× magnification of the side surface, and 25× and 1000× magnification of fractured surface.

No voids or defects were observed on the surface of HDPE/ 4.0 wt. % and HDPE/ 8.0 wt. % biochar samples. This indicated that the 3D printing settings were appropriate. The failure to use proper 3D printing settings to build parts affects the voids and defects in their structures

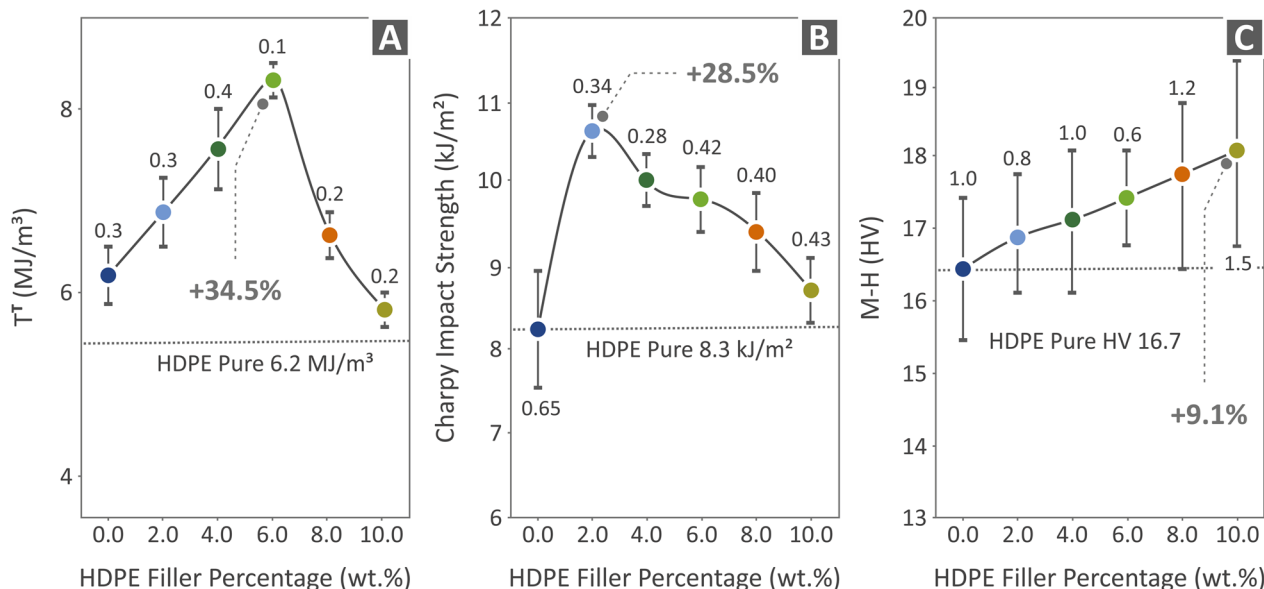


**Fig. 11** Results from the specimens' tests (pure HDPE and all HDPE/ biochar composites, i.e., 2.0, 4.0, 6.0, 8.0, and 10.0 wt. %) **A** tensile toughness, **B** Charpy impact strength, and **C** microhardness

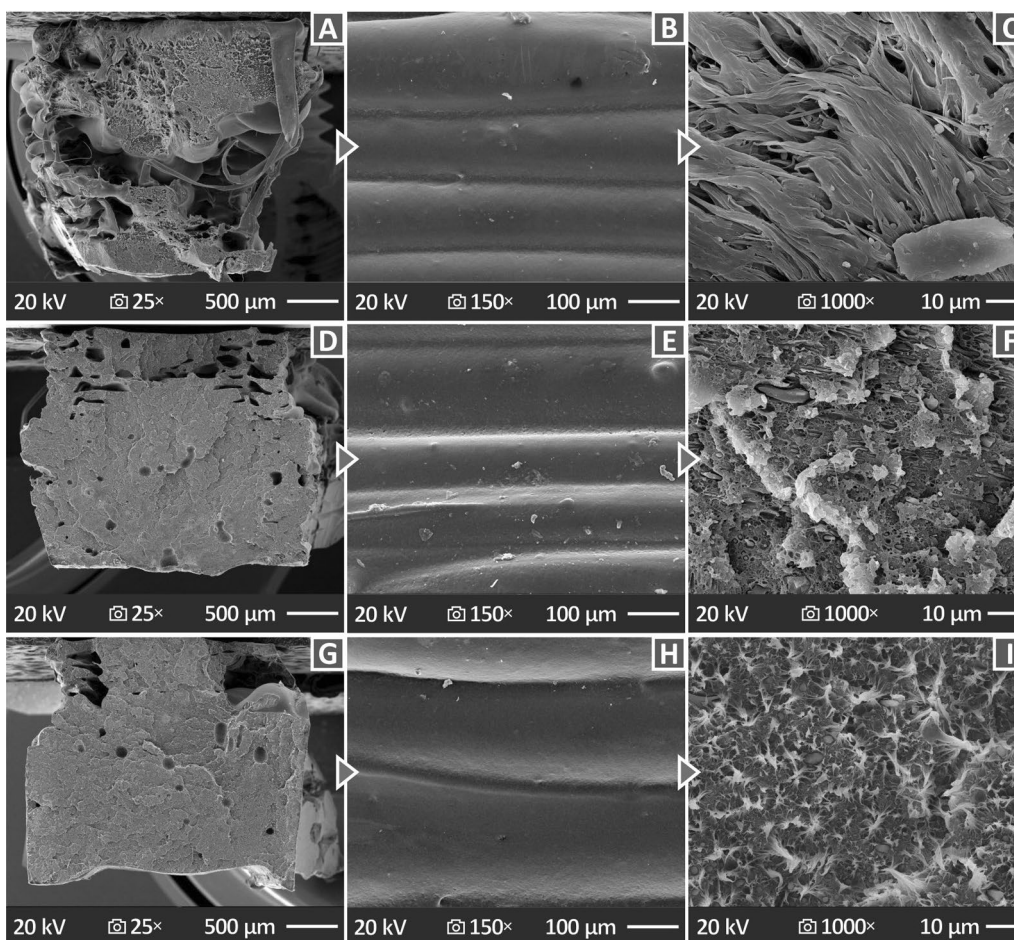


**Fig. 12** SEM images of HDPE pure **A** fracture surface at 25 $\times$  magnification, **B** side surface at 150 $\times$  magnification, **C** fracture surface at 1000 $\times$  magnification, HDPE/ 4.0 wt. % biochar **D** fracture surface at 25 $\times$  magnification, **E** side surface at 150 $\times$  magnification, **F** fracture surface at 1000 $\times$  magnification, HDPE/ 8.0 wt. % biochar **G** fracture surface at 25 $\times$  magnification, **H** side surface at 150 $\times$  magnification, and **I** fracture surface at 1000 $\times$  magnification

(Jang et al. 2021; Yang et al. 2021). The HDPE/ 8.0 wt. % biochar showed an irregular 3D structure, indicating that the 3D printing settings required adjustment to higher biochar loadings, to achieve a better 3D printing quality and probably a better mechanical performance. All samples were 3D printed with the same settings as the pure HDPE to obtain comparable results.

However, the fractured structure images revealed many pores and voids, particularly in the case of pure HDPE, where a less compact and regular structure can be observed. From a higher magnification (1000 $\times$ ), a more fibrous form was observed in the case of pure HDPE, while HDPE/ 4.0 wt. % and HDPE/ 8.0 wt. % biochar samples showed less deformation indicating a more brittle fracture mechanism at this microscale level, although the samples overall failed at higher strain values compared to pure HDPE.

Figure 13A, B and C present SEM images of HDPE/ 10.0 wt. % biochar at 25 $\times$  and 1000 $\times$  and 15,000 $\times$  magnifications, respectively. Figure 13D and E present side-surface SEM images of HDPE/ 10.0 wt. % biochar at 30 $\times$  and 150 $\times$  magnifications respectively, while Fig. 13F shows an EDS mapping for the carbon element of HDPE/ 10.0 wt. % biochar. A uniform dispersion of carbon was observed, indicating that the dispersion of biochar in the composites, even at this loading, was sufficient. The side surface of HDPE/ 10.0 wt. % biochar showed a few small defects, but the layering, appeared to be uniform, while the fractured surface images of the same composite were porous. In the EDS mapping, the distribution of C in the observation region was uniform, and even in the higher-magnification images, no agglomeration of biochar particles was observed,

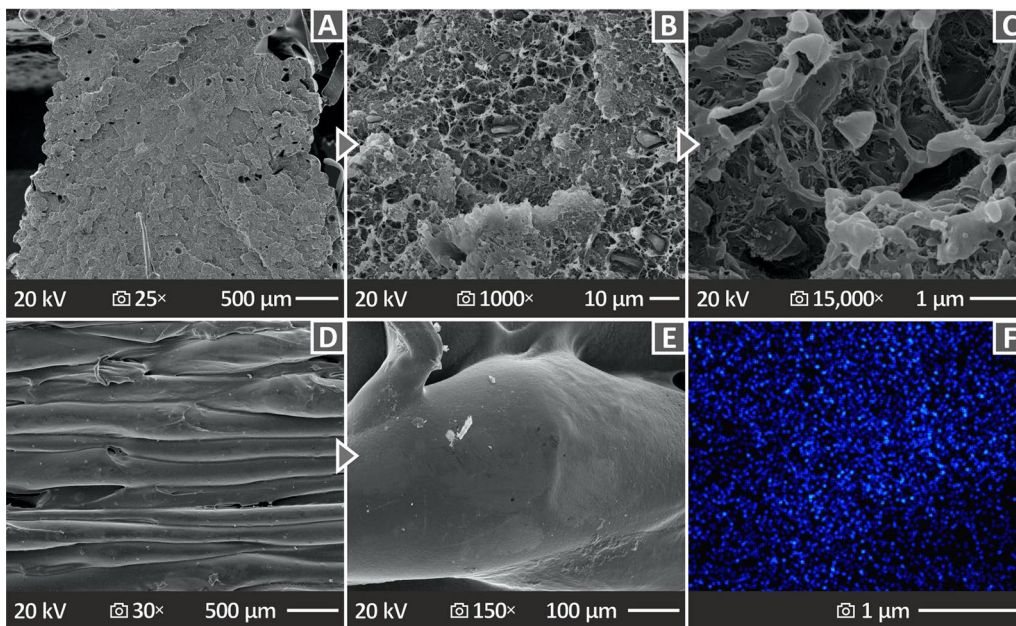


**Fig. 13** **A** SEM fracture surface image of HDPE/ 10.0 wt. % biochar at 25× magnification, **B** SEM fracture surface image of HDPE/ 10.0 wt. % biochar at 1000× magnification **C** SEM fracture surface image of HDPE/ 10.0 wt. % biochar at 15,000× magnification, **D** SEM side surface image of HDPE/ 10.0 wt. % biochar at 30× magnification, **E** SEM side surface image of HDPE/ 10.0 wt. % biochar at 150× magnification, and **F** MAP image of HDPE/ 10.0 wt. % biochar

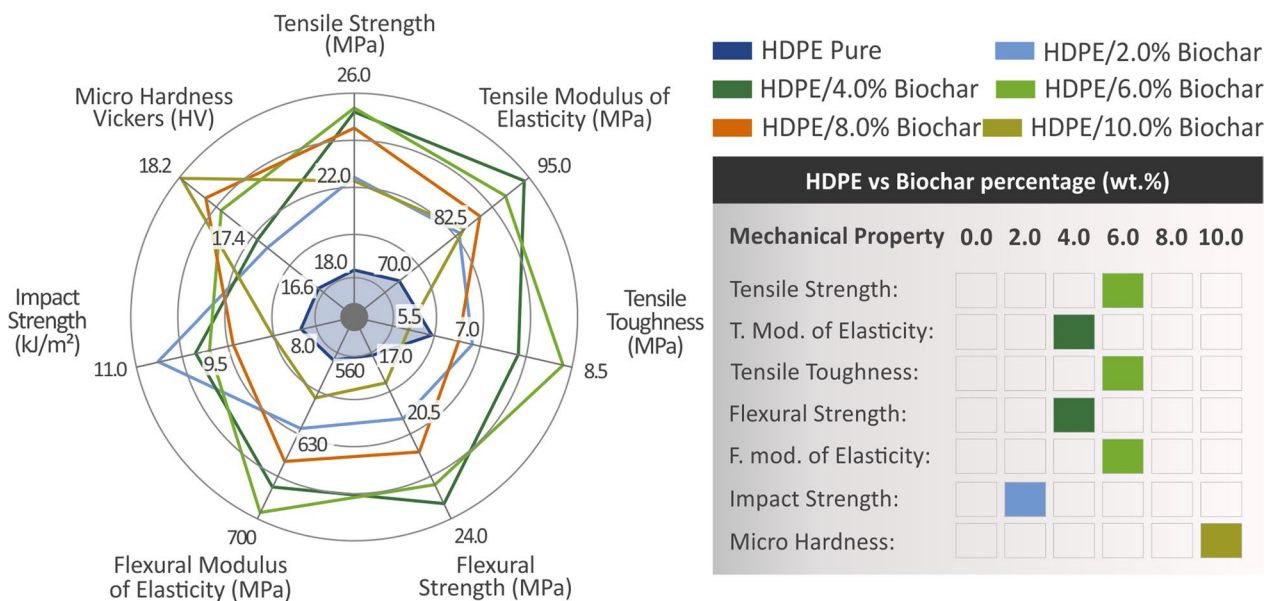


**Fig. 14** Summary of the results arising from the conducted mechanical tests (left side), along with the presentation of the filler loading in the composites that achieved the highest values of each mechanical property (right side)

indicating that the composite preparation process was sufficient for the specific composites studied herein.

#### 4 Discussion

For this investigation, HDPE was utilized along with biochar (which was derived from olive tree pruning) as a filler to study the mechanical performance of the produced composites and evaluate the effect of sustainable, eco-friendly biochar as a reinforcement agent for the popular HDPE thermoplastic in MEX 3D printing. Five composites were created namely HDPE/ 2.0 wt. % biochar, HDPE/ 4.0 wt. % biochar, HDPE/ 6.0 wt. % biochar, HDPE/ 8.0 wt. % biochar and HDPE/ 10.0 wt. % biochar. The tensile and flexural strengths, tensile and flexural moduli of elasticity, tensile toughness, Charpy impact strength, and microhardness were evaluated using mechanical tests. The left side of Fig. 14 presents a summary of the results obtained from all mechanical tests conducted. The right side of Fig. 14 highlights which biochar loading exhibited the highest values for each mechanical property. Biochar as a filler sufficiently reinforced HDPE. The results showed that the filler improved the mechanical properties of HDPE/biochar nanocomposites. The reinforcing mechanism of the addition of carbon-based fillers in the polymeric matrix is related to different phenomena, such as the chemical bonding between the filler and matrix and the interfacial shear stress, among others (Li et al. 2007; Han et al. 2023).

When the biochar concentration was higher than 6.0 wt. %, the mechanical properties of the composites deteriorated, although even the highest loaded composite tested (10.0 wt. %) showed higher values of the mechanical properties than the unfilled HDPE (approximately 17% higher tensile strength). This indicates that the biochar starts to saturate the matrix, and aggregates are formed, which negatively affects the mechanical properties of the composites (Li et al. 2020; Mostafa et al. 2020; Tamayo-Vegas et al. 2022; Shah et al. 2023b). Particle agglomeration may act as a fracture point in the composite owing to the stress concentration effect (Ferreira et al. 2019). Therefore, considering the limitations of 3D printing regarding biochar loading, higher values of mechanical properties are not expected to be achieved at loadings higher than 10.0 wt. %. The exact saturation threshold was not identified in this study, because it was not within its scope. Overall, with the preparation process followed for the composites in MEX 3D printing, the 6.0 wt. % filled composite achieved the most improved mechanical performance, with the highest values in the mechanical properties mentioned above and high values in the remaining mechanical properties. Notably, electrical characterization of the samples clearly showed that at biochar contents higher than 8.0

wt. %, the dc-conductivity rapidly increases by nearly 5 orders of magnitude, suggesting the existence of a critical filler concentration above which the composite exhibits enhanced electrical behavior. This percolation threshold is close to the optimum filler content (6.0 wt. %), where the HDPE/biochar composite also exhibits improved mechanical behavior.

Inspection of the morphological characteristics of the samples using SEM and EDS showed that the composites failed with lower deformation on the fracture surface. At the same time, they exhibited a more solid structure with fewer pores and internal voids than pure HDPE. This difference in the structure, which was revealed during the SEM inspection, may have contributed to the increased mechanical performance of the composites. However, the internal voids in pure HDPE may have increased during the failure of the samples in the tests. With the process followed for the preparation of the composites, no biochar particle aggregation was observed, even for the highest-loaded composite. EDS mapping also showed a uniform distribution of C in the observed region, verifying this assumption. This was also verified by small deviations in the mechanical tests, which indicated a uniform material composition in the tested samples. These observations further confirmed that rod mill grinding of raw biochar satisfactorily reduced the particle size of the material, ensuring uniform contact with the HDPE particles during the mixing process. At the industrial scale, the average particle size of carbon black additives in HDPE typically ranges between 20 and 70 nm. However, reducing the particle size to exceptionally small values requires energy-intensive milling. Therefore, using biochar with particle sizes in the 10–50  $\mu\text{m}$  micrometer range is advantageous from an energy perspective.

From the side surface SEM images, at high biochar concentrations, the layer formation worsened. This shows that the 3D printing settings should be fine-tuned at these loadings, with differences attributed to the effect of biochar on the rheological behavior of the HDPE polymer. Optimized 3D printing settings for higher-loaded composites are expected to further improve the mechanical performances of these samples. However, the 3D printing settings were kept the same for all the fabricated samples to obtain comparable results. Nevertheless, biochar loadings up to 70% in HDPE have been reported in the literature, although 3D printing has not been used (Zhang et al. 2020b, c). Regarding the thermal behavior of the composites, the TGA and DSC results showed that the addition of biochar did not significantly affect the thermal properties of the HDPE thermoplastic. At the same time, TGA ensured that the extrusion and 3D printed temperatures used did not cause any degradation in the composites, which would have affected the mechanical



test results. Comparing the TGA responses of the pure HDPE and HDPE/biochar composites, the acute degradation of the polymer occurred at similar temperatures (Al-Bayaty et al. 2020). However, the initial degradation at approximately 320 °C before the acute degradation of HDPE at temperatures much higher than 400 °C was not observed in this study (Al-Bayaty et al. 2020). The addition of TiO<sub>2</sub> (Vidakis et al. 2022a) and zinc oxide (ZnO) (Vidakis et al. 2022b) to the HDPE matrix for the preparation of composites for the MEX 3D printing method had a similar effect on the response of the HDPE matrix to the temperature increase in the current study. Acute degradation of the polymer was not significantly affected by the addition of fillers.

A previous study investigated similar mixtures of materials, such as biochar with high-density polyethylene composites, at concentrations lower than those used in this study (0.5, 1.0, 1.5, and 2.0 wt. %). The composites exhibited improved thermal properties compared with those of pure HDPE (Zhang et al. 2020b). In another study (Idrees et al. 2018), efforts were made to create low-cost, sustainable biochar-recycled polyethylene terephthalate (PET) composites with improved mechanical and thermal properties. Biochar was developed through the pyrolysis of packaging waste. Results indicated that the utilization of biochar was effective for reinforcing the mechanical, thermal, and dynamic properties of the composites as also happened in the study herein.

In another study, where biochar-reinforced polymers were investigated, it was found that the impact strength increased by uniformly increasing the particle loading, whereas the tensile strength was reduced as the particle loading increased (Richard et al. 2016). Biochar derived from cashew nutshell waste (CNSL) through pyrolysis was utilized as reinforcement for unsaturated polyester resins. Specimens of the produced composites were fabricated and subjected to tensile, flexural, and impact

strength tests, all of which showed great improvement in the case of 10.0 wt. % biochar composite (Sundarakannan et al. 2020).

In an additional investigation, biochar from plantain stalk fiber was utilized as a reinforcement for polystyrene to create composites and to examine their thermal and functional properties. It was proven that the 30% filler (a much higher biochar loading than the study’s study) presented the optimum thermal stability (Onifade et al. 2020). Biochar prepared through the pyrolysis of agricultural waste was utilized along with styrene butadiene (SBR), and various composites with different filler concentrations were fabricated (Abd El-Aziz et al. 2022). The results showed that the tensile strength of the SBR decreased with the addition of biochar, which is in contrast to the results for the response of HDPE/biochar in this study. None of the aforementioned studies were carried out on 3D printed parts, and some did not aim to reinforce the polymeric matrices. Composites were prepared using methods different from those used in this study. Additionally, biochar was prepared from different natural resources compared to the current study, and in some cases, using a different production method. Therefore, the results cannot be directly correlated. In MEX 3D printing, biochar is introduced into the PLA polymer for the development of composites using a method similar to that implemented herein (Vidakis et al. 2023a). The reinforcing effect of the PLA polymer was slightly lower than that observed in this study. However, research on biochar for 3D printing is limited.

Carbon-based additives have been incorporated into the HDPE in MEX 3D printing, such as carbon fibers (Borkar et al. 2022) and multiwall carbon nanotubes (MWNT) (Kumar et al. 2022). The effect of carbon fibers as fillers is different from that of particles, with carbon fibers reinforcing the matrices in a greater way than particles. In this study (Borkar et al. 2022), a loading of 11.2

**Table 1** Comparison of the findings of the study with the literature

Matrix	Additive	Optimum filler loading (wt. %)	3D printing	Tensile strength (% increase)	Flexural strength (% increase)	References
HDPE	Biochar	6.0	Yes	37.8	35.9	Current study
PLA	Biochar	4.0	Yes	20.9	14.1	Vidakis et al. (2023a)
PET	Biochar	0.5	Yes	~20	–	Idrees et al. (2018)
HDPE	Biochar	0.5	No	~29	> 100%	Zhang et al. (2020b)
Polyester resin	Biochar	10	No	21	41	Sundarakannan et al. (2020)
HDPE	CF *	11.2	Yes	30	–	Borkar et al. (2022)
HDPE	TiO <sub>2</sub>	10.0	Yes	28.5	77.6	Vidakis et al. (2022a)
HDPE	Zn	2.5	Yes	53.8 (10 wt. %)	~400%	Vidakis et al. (2022b)
HDPE	MWCNT **	5.0	Yes	~11	~19%	Kumar et al. (2022)

\*Carbon fibers, \*\*multi-wall carbon nanotubes

wt. % the tensile strength was approximately 30%, which is comparable to that of the current study. However, with carbon fiber as an additive, loadings of up to 29.5 wt. % were possible, significantly increasing the mechanical performance of the samples in this case (+160.7%). Regarding multiwall carbon nanotubes (Kumar et al. 2022), composites with loadings up to 5.0 wt. % were prepared. The tensile strength increased with the increase in MWNT in the composites, with the highest increase achieved at the highest loading of 5.0 wt. % tested. An increase of approximately 11% was achieved in the tensile strength of the 3D-printed samples. The flexural strength, increased by approximately 18% compared to that of pure HDPE. The current research reports significantly higher improvements in both the tensile and flexural strengths compared to (Kumar et al. 2022). It should be noted that the tensile and flexural strength values for pure HDPE are remarkably similar in both studies; therefore, the reinforcement effect can be safely compared between these two studies [current study and (Kumar et al. 2022)], especially considering that the composites were prepared using a similar method in the studies. Additionally, the introduction of MWNT into the HDPE matrix reduced the MFI of the rheological properties, similar to the current study, in which the same effect was observed. A comparison of the findings presented herein with those of some of the most relevant studies is presented in Table 1.

## 5 Conclusions

In this study, the reinforcing properties of biochar as a filler for HDPE in the MEX 3D printing method were investigated through a sequence of mechanical tests conducted using five different filler concentrations (2.0, 4.0, 6.0, 8.0, 10.0 wt. %). Pure HDPE was used as a control. HDPE/ 4.0 wt. % biochar and HDPE/ 6.0 wt. % biochar showed the highest improvement. Tensile strength (37.8% improvement) and toughness (35.5% improvement), as well as flexural modulus of elasticity (22.3% improvement), showed the highest results in the case of HDPE/ 6.0 wt. % biochar, while the tensile modulus of elasticity (29.5% improvement), and flexural strength (35.9% improvement), were higher in the HDPE/ 4.0 wt. % biochar composite. Moreover, the impact strength was improved in the case of HDPE/ 2.0 wt. % biochar (28.5% improvement), and microhardness in the case of HDPE/ 10.0 wt. % biochar (9.1% improvement). Overall, the 6.0 wt. % biochar can be considered the optimum loading in the study. Thermal, structural, rheological, electrical, and morphological studies were performed to fully characterize the prepared composites and ensure their overall performance and merits, justifying the findings. The introduction of biochar into

the prepared composites improved the electrical conductivity of HDPE by several orders of magnitude, indicating that it can also be considered a valuable additive for improving the electrical properties of polymers. The biochar used as a filler was prepared from olive trees, with a specific grade rarely presented in the literature, especially in 3D printing. Overall, this study proved that utilizing eco-friendly biochar as a reinforcement for HDPE in MEX 3D printing can be effective in terms of mechanical performance and benefit various AM applications. Therefore, biochar can be used as a filler to improve the performance of HDPE in MEX 3D printing, having obvious advantages over common chemically produced fillers, such as the fact that it is an eco-friendly and sustainable filler. Its performance is comparable to that of existing fillers, providing electrical conductivity characteristics simultaneously owing to its carbon-based nature, with improved performance in this area compared to other composites with different polymeric matrices. These findings are advantageous for direct industrial applications in fields where a popular HDPE polymer is used.

## Supplementary Information

The online version contains supplementary material available at <https://doi.org/10.1007/s42773-024-00314-5>.

**Additional file 1.** Supplementary material.

## Acknowledgements

The authors would like to thank the Institute of Electronic Structure and Laser of the Foundation for Research and Technology-Hellas (IESL-FORTH) and, in particular, Ms. Aleka Manousaki for taking the SEM images presented in this work, and the Photonic Phononic and Meta-Materials Laboratory for sharing the Raman Instrumentation.

## Author contributions

NV: Conceptualization, methodology, resources, supervision, project administration; MP: Methodology, formal analysis, writing—original draft preparation, writing—review, and editing; DK: investigation, methodology, validation, formal analysis; NM: supervision, project administration; EM: validation, methodology; VS: formal analysis, writing—original draft preparation; NB: validation, formal analysis; VP: Visualization, Validation; MS: writing—original draft preparation, investigation; AA: data curation, visualization. The manuscript was written with contributions from all the authors. All the authors approved the final version of the manuscript.

## Funding

This study did not receive any external funding.

## Data availability

The raw/processed data required to reproduce these findings cannot be shared because of technical and time limitations.

## Declarations

### Competing interests

The authors declare that they have no known competing financial interests or personal relationships that could have influenced the work reported in this paper.

**Author details**

<sup>1</sup>Department of Mechanical Engineering, Hellenic Mediterranean University, 71410 Heraklion, Greece. <sup>2</sup>Department of Electronic Engineering, Hellenic Mediterranean University, 73133 Chania, Greece. <sup>3</sup>Physical Metallurgy Laboratory, Mechanical Engineering Department, School of Engineering, Aristotle University of Thessaloniki, 54124 Thessaloniki, Greece. <sup>4</sup>Centre for Research and Development of Advanced Materials (CERDAM), Center for Interdisciplinary Research and Innovation, Balkan Centre, Building B', 10th Km Thessaloniki-Thermi Road, 57001 Thessaloniki, Greece. <sup>5</sup>Department of Industrial Design and Production Engineering, University of West Attica, 122 43 Athens, Greece. <sup>6</sup>Institute of Electronic Structure and Laser, Foundation for Research and Technology–Hellas, N. Plastira 100M, 70013 Heraklion, Greece.

Received: 25 November 2023 Revised: 21 February 2024 Accepted: 23 February 2024

Published online: 09 April 2024

**References**

- Abd El-Aziz ME, Shafik ES, Tawfic ML, Morsi SMM (2022) Biochar from waste agriculture as reinforcement filler for styrene/butadiene rubber. *Polym Compos* 43(3):1295–1304. <https://doi.org/10.1002/pc.26448>
- Ahmad M, Rajapaksha AU, Lim JE, Zhang M, Bolan N, Mohan D, Vithanage M, Lee SS, Ok YS (2014) Biochar as a sorbent for contaminant management in soil and water: a review. *Chemosphere* 99:19–33. <https://doi.org/10.1016/j.chemosphere.2013.10.071>
- Ahmed MJ, Hameed BH (2020) Insight into the co-pyrolysis of different blended feedstocks to biochar for the adsorption of organic and inorganic pollutants: a review. *J Clean Prod* 265:121762. <https://doi.org/10.1016/j.jclepro.2020.121762>
- Al-Bayaty SA, Al-Uqaily RAH, Hameed S (2020) Study of thermal degradation kinetics of high density polyethylene (HDPE) by using TGA technique. *AIIP Conf Proc* 2290(1):20001. <https://doi.org/10.1063/5.0027503>
- Amalina F, Razak ASA, Krishnan S, Sulaiman H, Zularisam AW, Nasrullah M (2022) Biochar production techniques utilizing biomass waste-derived materials and environmental applications—a review. *J Hazardous Mater Adv* 7:100134. <https://doi.org/10.1016/j.hazadv.2022.100134>
- Aup-Ngoen K, Noipitak M (2020) Effect of carbon-rich biochar on mechanical properties of PLA-biochar composites. *Sustain Chem Pharm* 15:100204. <https://doi.org/10.1016/j.scp.2019.100204>
- Awad SA (2021) Swelling, thermal and mechanical characterizations of high-density polyethylene/ recycled biochar composites. *J Turk Chem Soc Sect A Chem* 8(4):1137–1144. <https://doi.org/10.18596/jotcsa.984583>
- Beydoun K, Klankermayer J (2020) Efficient plastic waste recycling to value-added products by integrated biomass processing. *Chemoschem* 13(3):488–492. <https://doi.org/10.1002/cssc.201902880>
- Borkar A, Hendlmeier A, Simon Z, Randall JD, Stojcevski F, Henderson LC (2022) A comparison of mechanical properties of recycled high-density polyethylene/waste carbon fiber via injection molding and 3D printing. *Polym Compos* 43(4):2408–2418. <https://doi.org/10.1002/pc.26550>
- Brigandi PJ, Cogen JM, Pearson RA (2014) Electrically conductive multiphase polymer blend carbon-based composites. *Polym Eng Sci* 54(1):1–16. <https://doi.org/10.1002/pen.23530>
- Cuevas M, Martínez-Cartas ML, Pérez-Villarejo L, Hernández L, García-Martín JF, Sánchez S (2019) Drying kinetics and effective water diffusivities in olive stone and olive-tree pruning. *Renew Energy* 132:911–920. <https://doi.org/10.1016/j.renene.2018.08.053>
- Dahal RK, Acharya B, Saha G, Bissessur R, Dutta A, Farooque A (2019) Biochar as a filler in glassfiber reinforced composites: experimental study of thermal and mechanical properties. *Compos B Eng* 175:107169. <https://doi.org/10.1016/j.compositesb.2019.107169>
- Das O, Sarmah AK, Bhattacharyya D (2015a) A novel approach in organic waste utilization through biochar addition in wood/polypropylene composites. *Waste Manag* 38:132–140. <https://doi.org/10.1016/j.wasman.2015.01.015>
- Das O, Sarmah AK, Bhattacharyya D (2015b) Structure–mechanics property relationship of waste derived biochars. *Sci Total Environ* 538:611–620. <https://doi.org/10.1016/j.scitotenv.2015.08.073>
- Das O, Bhattacharyya D, Hui D, Lau K-T (2016a) Mechanical and flammability characterisations of biochar/polypropylene biocomposites. *Compos B Eng* 106:120–128. <https://doi.org/10.1016/j.compositesb.2016.09.020>
- Das O, Bhattacharyya D, Sarmah AK (2016b) Sustainable eco-composites obtained from waste derived biochar: a consideration in performance properties, production costs, and environmental impact. *J Clean Prod* 129:159–168. <https://doi.org/10.1016/j.jclepro.2016.04.088>
- Das O, Kim NK, Kalamkarov AL, Sarmah AK, Bhattacharyya D (2017a) Biochar to the rescue: Balancing the fire performance and mechanical properties of polypropylene composites. *Polym Degrad Stab* 144:485–496. <https://doi.org/10.1016/j.polymdegradstab.2017.09.006>
- Das O, Kim NK, Sarmah AK, Bhattacharyya D (2017b) Development of waste based biochar/wool hybrid biocomposites: flammability characteristics and mechanical properties. *J Clean Prod* 144:79–89. <https://doi.org/10.1016/j.jclepro.2016.12.155>
- Das D, Bordoloi U, Muigai HH, Kalita P (2020) A novel form stable PCM based bio composite material for solar thermal energy storage applications. *J Energy Storage* 30:101403. <https://doi.org/10.1016/j.est.2020.101403>
- Das C, Tamrakar S, Kiziltas A, Xie X (2021) Incorporation of biochar to improve mechanical thermal and electrical properties of polymer composites. *Polymers (basel)*. <https://doi.org/10.3390/polym13162663>
- de Sousa DV, Guimarães LM, Félix JF, Ker JC, Schaefer CERG, Rodet MJ (2020) Dynamic of the structural alteration of biochar in ancient Anthrosol over a long timescale by Raman spectroscopy. *PLoS ONE* 15(3):e0229447
- DeVallance DB, Oporto GS, Quigley P (2015) Investigation of hardwood biochar as a replacement for wood flour in wood–polypropylene composites. *J Elastomers Plast* 48(6):510–522. <https://doi.org/10.1177/0095244315589655>
- Dusunceli N, Colak OU (2008) The effects of manufacturing techniques on viscoelastic and viscoplastic behavior of high density polyethylene (HDPE). *Mater Des* 29(6):1117–1124. <https://doi.org/10.1016/j.matdes.2007.06.003>
- Ferreira GF, Pierozzi M, Fingolo AC, da Silva WP, Strauss M (2019) Tuning sugarcane bagasse biochar into a potential carbon black substitute for polyethylene composites. *J Polym Environ* 27(8):1735–1745. <https://doi.org/10.1007/s10924-019-01468-1>
- Gabhi RS, Kirk DW, Jia CQ (2017) Preliminary investigation of electrical conductivity of monolithic biochar. *Carbon N Y* 116:435–442. <https://doi.org/10.1016/j.carbon.2017.01.069>
- García Martín JF, Cuevas M, Feng C-H, Álvarez Mateos P, Torres García M, Sánchez S (2020) Energetic valorisation of olive biomass: olive-tree pruning, olive stones and pomaces. *Processes*. <https://doi.org/10.3390/pr8050511>
- Ghoshal S (2017) Polymer/carbon nanotubes (CNT) nanocomposites processing using additive manufacturing (three-dimensional printing) technique: an overview. *Fibers*. <https://doi.org/10.3390/fib5040040>
- Giorcelli M, Khan A, Pugno NM, Rosso C, Tagliaferro A (2019) Biochar as a cheap and environmental friendly filler able to improve polymer mechanical properties. *Biomass Bioenergy* 120:219–223. <https://doi.org/10.1016/j.biombioe.2018.11.036>
- Gulrez SKH, Ali Mohsin ME, Shaikh H, Anis A, Pulose AM, Yadav MK, Qua EHP, Al-Zahrani SM (2014) A review on electrically conductive polypropylene and polyethylene. *Polym Compos* 35(5):900–914. <https://doi.org/10.1002/pc.22734>
- Han W, Zhou J, Shi Q (2023) Research progress on enhancement mechanism and mechanical properties of FRP composites reinforced with graphene and carbon nanotubes. *Alexandria Eng J* 64:541–579. <https://doi.org/10.1016/j.aej.2022.09.019>
- Idrees M, Jeelani S, Rangari V (2018) Three-dimensional-printed sustainable biochar-recycled PET composites. *ACS Sustain Chem Eng* 6(11):13940–13948. <https://doi.org/10.1021/acssuschemeng.8b02283>
- Ikram S, Das O, Bhattacharyya D (2016) A parametric study of mechanical and flammability properties of biochar reinforced polypropylene composites. *Compos Part A Appl Sci Manuf* 91:177–188. <https://doi.org/10.1016/j.compositesa.2016.10.010>
- Jang S, Boddorff A, Jang DJ, Lloyd J, Wagner K, Thadhani N, Brettmann B (2021) Effect of material extrusion process parameters on filament geometry and inter-filament voids in as-fabricated high solids loaded polymer composites. *Addit Manuf* 47:102313. <https://doi.org/10.1016/j.addma.2021.102313>
- Junk S, Dörner M, Fleig C (2021) Additive manufacturing of continuous carbon fiber-reinforced plastic components. In: Scholz SG, Howlett RJ, Setchi R (eds) *Sustainable design and manufacturing 2020*. Springer Singapore, Singapore, pp 149–159

- Khan A, Savi P, Quaranta S, Rovere M, Giorcelli M, Tagliaferro A, Rosso C, Jia CQ (2017) Low-cost carbon fillers to improve mechanical properties and conductivity of epoxy composites. *Polymers* (basel). <https://doi.org/10.3390/polym9120642>
- Khushnood RA, Ahmad S, Savi P, Tulliani J-M, Giorcelli M, Ferro GA (2015) Improvement in electromagnetic interference shielding effectiveness of cement composites using carbonaceous nano/micro inerts. *Constr Build Mater* 85:208–216. <https://doi.org/10.1016/j.conbuildmat.2015.03.069>
- Kostenidou E, Kaltsounoudis C, Tsiflikiotou M, Louvaris E, Russell LM, Pandis SN (2013) Burning of olive tree branches: a major organic aerosol source in the Mediterranean. *Atmos Chem Phys* 13(17):8797–8811. <https://doi.org/10.5194/acp-13-8797-2013>
- Krupa I, Novák I, Chodák I (2004) Electrically and thermally conductive polyethylene/graphite composites and their mechanical properties. *Synth Met* 145(2):245–252. <https://doi.org/10.1016/j.synthmet.2004.05.007>
- Kumar S, Panda AK, Singh RK (2011) A review on tertiary recycling of high-density polyethylene to fuel. *Resour Conserv Recycl* 55(11):893–910. <https://doi.org/10.1016/j.resconrec.2011.05.005>
- Kumar S, Ramesh MR, Doddamani M, Rangappa SM, Siengchin S (2022) Mechanical characterization of 3D printed MWCNTs/HDPE nanocomposites. *Polym Test* 114:107703. <https://doi.org/10.1016/j.polymertesting.2022.107703>
- Lee JW, Hawkins B, Li X, Day DM (2013) Biochar fertilizer for soil amendment and carbon sequestration. In: Lee JW (ed) *Advanced biofuels and bioproducts*. Springer New York, New York, pp 57–68
- Lehmann J, Rillig MC, Thies J, Masiello CA, Hockaday WC, Crowley D (2011) Biochar effects on soil biota—a review. *Soil Biol Biochem* 43(9):1812–1836. <https://doi.org/10.1016/j.soilbio.2011.04.022>
- Li S, Li D (2014) Carbon fiber reinforced highly filled charcoal powder/ultra high molecular weight polyethylene composites. *Mater Lett* 134:99–102. <https://doi.org/10.1016/j.matlet.2014.07.081>
- Li X, Gao H, Scrivens WA, Fei D, Xu X, Sutton MA, Reynolds AP, Myrick ML (2007) Reinforcing mechanisms of single-walled carbon nanotube-reinforced polymer composites. *J Nanosci Nanotechnol* 7(7):2309–2317. <https://doi.org/10.1166/jnn.2007.410>
- Li X, Song Y, Bian Y, Wang F, Gu C, Yang X, Jiang X (2019) Effects of root exudates on the sorption of polycyclic aromatic hydrocarbons onto biochar. *Environ Pollut Bioavailab* 31(1):156–165. <https://doi.org/10.1080/26395940.2019.1593054>
- Li Z, Fan M, Zhong Z, Du B (2020) Coupling effect of molecular chain displacement and carrier trap characteristics on DC breakdown of HDPE/LDPE blend insulation. *Polymers* (basel). <https://doi.org/10.3390/polym1230589>
- Linares A, Canalda JC, Cagiao ME, García-Gutiérrez MC, Nogales A, Martín-Gullón I, Vera J, Ezquerro TA (2008) Broad-band electrical conductivity of high density polyethylene nanocomposites with carbon nanoadditives: multiwall carbon nanotubes and carbon nanofibers. *Macromolecules* 41(19):7090–7097. <https://doi.org/10.1021/ma801410j>
- Mandal S, Adhikari S, Ma H, Kim D-H, Bai Y, Hou D (2020) Progress and future prospects in biochar composites: application and reflection in the soil environment. *Crit Rev Environ Sci Technol*. <https://doi.org/10.1080/10643389.2020.1713030>
- Manyà JJ (2012) Pyrolysis for biochar purposes: a review to establish current knowledge gaps and research needs. *Environ Sci Technol* 46(15):7939–7954. <https://doi.org/10.1021/es301029g>
- Matykiewicz D (2020) Biochar as an effective filler of carbon fiber reinforced bio-epoxy composites. *Processes*. <https://doi.org/10.3390/pr8060724>
- Mazzanti V, Malagutti L, Mollica F (2019) FDM 3D printing of polymers containing natural fillers: a review of their mechanical properties. *Polymers* (basel). <https://doi.org/10.3390/polym11071094>
- Meyer S, Glaser B, Quicker P (2011) Technical, economical, and climate-related aspects of biochar production technologies: a literature review. *Environ Sci Technol* 45(22):9473–9483. <https://doi.org/10.1021/es201792c>
- Mostafa SA, Faried AS, Farghali AA, El-Deeb MM, Tawfik TA, Majer S, Abd Elrahman M (2020) Influence of nanoparticles from waste materials on mechanical properties, durability and microstructure of UHPC. *Materials*. <https://doi.org/10.3390/ma13204530>
- Musa ET, Hamza A, Ahmed AS (2017) Investigation of the mechanical and morphological properties of high-density polyethylene (hdpe)/leather waste composites. *IOSR J Appl Chem* 10(01):48–58. <https://doi.org/10.9790/5736-1001014858>
- Nan N, DeVallance DB, Xie X, Wang J (2015) The effect of bio-carbon addition on the electrical, mechanical, and thermal properties of polyvinyl alcohol/biochar composites. *J Compos Mater* 50(9):1161–1168. <https://doi.org/10.1177/0021998315589770>
- Nanda S, Dalai AK, Berruti F, Kozinski JA (2016) Biochar as an exceptional bioresource for energy, agronomy, carbon sequestration, activated carbon and specialty materials. *Waste Biomass Valorization* 7(2):201–235. <https://doi.org/10.1007/s12649-015-9459-z>
- Noman M, Sanginario A, Jagdale P, Castellino M, Demarchi D, Tagliaferro A (2014) Pyrolyzed bamboo electrode for electrogenerated chemiluminescence of Ru (bpy)<sub>3</sub>2+. *Electrochim Acta* 133:169–173. <https://doi.org/10.1016/j.electacta.2014.03.100>
- Pawlak A, Galeski A (2005) Plastic deformation of crystalline polymers: the role of cavitation and crystal plasticity. *Macromolecules* 38(23):9688–9697. <https://doi.org/10.1021/ma050842o>
- Petousis M, Michailidis N, Papadakis V, Mountakis N, Argyros A, Spiridakis M, Moutsopoulou A, Nasikas NK, Vidakis N (2023) The impact of the glass microparticles features on the engineering response of isotactic polypropylene in material extrusion 3D printing. *Mater Today Commun*. <https://doi.org/10.1016/j.mtcomm.2023.107204>
- Pk G, Tee KF, Gimbin J, Chin SC (2023) Biochar in cementitious material—a review on physical, chemical, mechanical, and durability properties. *AIMS Mater Sci* 10(3):405–425. <https://doi.org/10.3934/matrics.2023022>
- Richard S, Rajadurai JS, Manikandan V (2016) Influence of particle size and particle loading on mechanical and dielectric properties of biochar particulate-reinforced polymer nanocomposites. *Int J Polym Anal Charact* 21(6):462–477. <https://doi.org/10.1080/1023666X.2016.1168602>
- Romero-García JM, López-Linares JC, del Conteras M, Romero I, Castro E (2022) Exploitation of olive tree pruning biomass through hydrothermal pretreatments. *Ind Crops Prod* 176:114425. <https://doi.org/10.1016/j.indcrop.2021.114425>
- Saltas V, Vallianatos F, Gidarakos E (2013) Charge transport in diatomaceous earth studied by broadband dielectric spectroscopy. *Appl Clay Sci* 80–81:226–235. <https://doi.org/10.1016/j.clay.2013.02.028>
- Shah AR, Imdad A, Sadiq A, Malik RA, Alrobei H, Badruddin IA (2023a) Mechanical, thermal, and fire retardant properties of rice husk biochar reinforced recycled high-density polyethylene composite material. *Polymers* (basel). <https://doi.org/10.3390/polym15081827>
- Shen Y, Yoshikawa K (2013) Recent progresses in catalytic tar elimination during biomass gasification or pyrolysis—a review. *Renewable Sustain Energy Rev* 21:371–392. <https://doi.org/10.1016/j.rser.2012.12.062>
- Suljovrujic E, Micic M, Milicevic D (2013) Structural changes and dielectric relaxation behavior of uniaxially oriented high density polyethylene. *J Eng Fiber Fabr* 8(3):155892501300800320. <https://doi.org/10.1177/155892501300800316>
- Sundarakannan R, Arumugaprabu V, Manikandan V, Vigneshwaran S (2020) Mechanical property analysis of biochar derived from cashew nut shell waste reinforced polymer matrix. *Mater Res Express* 6(12):125349. <https://doi.org/10.1088/2053-1591/ab6197>
- Tamayo-Vegas S, Muhsan A, Liu C, Tarfaoui M, Lafdi K (2022) The effect of agglomeration on the electrical and mechanical properties of polymer matrix nanocomposites reinforced with carbon nanotubes. *Polymers* (basel). <https://doi.org/10.3390/polym14091842>
- Tareq R, Akter N, Azam MdS (2019) Chapter 10—biochars and biochar composites: low-cost adsorbents for environmental remediation. In: Ok YS, Tsang DCW, Bolan N, Novak JM (eds) *Biochar from biomass and waste*. Elsevier, pp 169–209
- Tomczyk A, Sokołowska Z, Boguta P (2020) Biochar physicochemical properties: pyrolysis temperature and feedstock kind effects. *Rev Environ Sci Biotechnol* 19(1):191–215. <https://doi.org/10.1007/s11157-020-09523-3>
- Tsubota T, Tsuchiya S, Kusumoto T, Kalderis D (2021) Assessment of biochar produced by flame-curtain pyrolysis as a precursor for the development of an efficient electric double-layer capacitor. *Energies* (basel) 14(22):7671. <https://doi.org/10.3390/en14227671>
- Väisänen T, Das O, Tomppo L (2017) A review on new bio-based constituents for natural fiber-polymer composites. *J Clean Prod* 149:582–596. <https://doi.org/10.1016/j.jclepro.2017.02.132>
- van de Werken N, Tekinalp H, Khanbolouki P, Ozcan S, Williams A, Tehrani M (2020) Additively manufactured carbon fiber-reinforced composites: state

- of the art and perspective. *Addit Manuf* 31:100962. <https://doi.org/10.1016/j.addma.2019.100962>
- Vidakis N, Petousis M, Kourinou M, Velidakis E, Mountakis N, Fischer-Griffiths PE, Grammatikos S, Tzounis L (2021a) Additive manufacturing of multifunctional polylactic acid (PLA)—multiwalled carbon nanotubes (MWCNTs) nanocomposites. *Nanocomposites* 7(1):184–199. <https://doi.org/10.1080/20550324.2021.2000231>
- Vidakis N, Petousis M, Maniadi A (2021b) Sustainable additive manufacturing: mechanical response of high-density polyethylene over multiple recycling processes. *Recycling* 6(1):1–14. <https://doi.org/10.3390/recycling6010004>
- Vidakis N, Petousis M, Tzounis L, Velidakis E, Mountakis N, Grammatikos SA (2021c) Polyamide 12/multiwalled carbon nanotube and carbon black nanocomposites manufactured by 3D printing fused filament fabrication: a comparison of the electrical, thermoelectric, and mechanical properties. *C (basel)* 7(2):38. <https://doi.org/10.3390/c7020038>
- Vidakis N, Petousis M, Velidakis E, Mountakis N, Fischer-Griffiths PE, Grammatikos S, Tzounis L (2021d) Fused filament fabrication three-dimensional printing multi-functional of polylactic acid/carbon black nanocomposites. *C (basel)* 7(3):52. <https://doi.org/10.3390/c7030052>
- Vidakis N, Petousis M, Velidakis E, Spiridaki M, Kechagias JD (2021e) Mechanical performance of fused filament fabricated and 3d-printed polycarbonate polymer and polycarbonate/ cellulose nanofiber nanocomposites. *Fibers* 9(11):74. <https://doi.org/10.3390/fib9110074>
- Vidakis N, Petousis M, Maniadi A, Papadakis V (2022a) MEX 3D printed HDPE / TiO<sub>2</sub> nanocomposites physical and mechanical properties investigation. *J Compos Sci* 6:209. <https://doi.org/10.3390/jcs6070209>
- Vidakis N, Petousis M, Maniadi A, Papadakis V (2022b) The impact of zinc oxide micro-powder filler on the physical and mechanical response of high-density polyethylene composites in material extrusion 3D printing. *J Compos Sci* 6(10):315. <https://doi.org/10.3390/jcs6100315>
- Vidakis N, Kalderis D, Petousis M, Maravelakis E, Mountakis N, Bolanakis N, Papadakis V (2023a) Biochar filler in MEX and VPP additive manufacturing: characterization and reinforcement effects in polylactic acid and standard grade resin matrices. *Biochar* 5(1):39. <https://doi.org/10.1007/s42773-023-00238-6>
- Vidakis N, Petousis M, Michailidis N, David C, Mountakis N, Papadakis V, Sfiakiotakis E, Sigris D, Spiridaki M, Argyros A (2023b) Optimized PCL/CNF bio-nanocomposites for medical bio-plotted applications: rheological, structural, and thermomechanical aspects. *Bioprinting* 36:e00311. <https://doi.org/10.1016/j.bprint.2023.e00311>
- Wang L, Ok YS, Tsang DCW, Alessi DS, Rinklebe J, Mašek O, Bolan NS, Hou D (2022) Biochar composites: emerging trends, field successes and sustainability implications. *Soil Use Manag* 38(1):14–38. <https://doi.org/10.1111/sum.12731>
- Wang Y, Liu X, Lan T, Yang Q, Cong S, Lin Y (2023) Corn stalk biochar-reinforced high-density polyethylene material: flame-retardant and anti-aging properties. *Fibers Polymers* 24(5):1771–1779. <https://doi.org/10.1007/s12221-023-00044-8>
- Yang D, Zhang H, Wu J, McCarthy ED (2021) Fibre flow and void formation in 3D printing of short-fibre reinforced thermoplastic composites: an experimental benchmark exercise. *Addit Manuf* 37:101686. <https://doi.org/10.1016/j.addma.2020.101686>
- Zhang Q, Cai H, Ren X, Kong L, Liu J, Jiang X (2017a) The dynamic mechanical analysis of highly filled rice husk biochar/high-density polyethylene composites. *Polymers (basel)*. <https://doi.org/10.3390/polym9110628>
- Zhang Q, Cai H, Yang K, Yi W (2017b) Effect of biochar on mechanical and flame retardant properties of wood—plastic composites. *Results Phys* 7:2391–2395. <https://doi.org/10.1016/j.rinp.2017.04.025>
- Zhang Q, Yi W, Li Z, Wang L, Cai H (2018) Mechanical properties of rice husk biochar reinforced high density polyethylene composites. *Polymers (basel)*. <https://doi.org/10.3390/polym10030286>
- Zhang Q, Cai H, Yi W, Lei H, Liu H, Wang W, Ruan R (2020a) Biocomposites from organic solid wastes derived biochars: a review. *Materials*. <https://doi.org/10.3390/ma13183923>
- Zhang Q, Xu H, Lu W, Zhang D, Ren X, Yu W, Wu J, Zhou L, Han X, Yi W, Lei H (2020b) Properties evaluation of biochar/high-density polyethylene composites: emphasizing the porous structure of biochar by activation. *Sci Total Environ* 737:139770. <https://doi.org/10.1016/j.scitotenv.2020.139770>
- Zhang Q, Zhang D, Lu W, Khan MU, Xu H, Yi W, Lei H, Huo E, Qian M, Zhao Y, Zou R (2020c) Production of high-density polyethylene biocomposites from rice husk biochar: effects of varying pyrolysis temperature. *Sci Total Environ* 738:139910. <https://doi.org/10.1016/j.scitotenv.2020.139910>
- Zhang Q, Zhang D, Xu H, Lu W, Ren X, Cai H, Lei H, Huo E, Zhao Y, Qian M, Lin X, Villota EM, Mateo W (2020d) Biochar filled high-density polyethylene composites with excellent properties: towards maximizing the utilization of agricultural wastes. *Ind Crops Prod* 146:112185. <https://doi.org/10.1016/j.indcrop.2020.112185>
- Ziegler D, Palmero P, Giorcelli M, Tagliaferro A, Tulliani J-M (2017) Biochars as innovative humidity sensing materials. *Chemosensors*. <https://doi.org/10.3390/chemosensors5040035>